Impact of channel models in MIMO OFDM for LTE

Aalborg University
May 2012

AALBORG UNIVERSITY

The Faculty of Engineering and Science
Department of Electronic Systems
Frederik Bajers Vej 7, 9220 Aalborg Øst
Phone: +45 99 40 86 00
http://es.aau.dk

Title:
Impact of channel models in MIMO OFDM for LTE
Theme:
Advanced software radio implementation
Project period:
September 1st 2011 – May 31st, 2012

Group number:
12gr1058
Group member(s):
Troels Jessen

Supervisors:
Gert F. Pedersen
Michael Knudsen
Christian Rom

Number of copies: 5
Number of pages: 56
Appended documents:
(4 appendices, 1 CD-ROM)
Total number of pages: 71
Finished: May 30th, 2012

Abstract:

In this report, a study of OFDM receiver algorithms for SISO, SIMO, and MIMO with SMUX and STBC is performed. The algorithms are compared using BER simulations in an uncorrelated Rayleigh fading channel. The system is extended to include Turbo coding and rate matching complying with the LTE standard, reaching a throughput of 11.2 bits/sec/Hz in an i.i.d. 2×2 Rayleigh fading channel. To maximize the advantage from the Turbo codes, a soft decision demodulator for M-PSK and M-QAM modulation constellations is developed.
Finally, the attention is brought to channel models with spatial correlation, created from statistics and geometry. A geometrically based channel model is developed and evaluated with respect to the Demmel Condition Number, and a comparison between this and the WINNER II channel model is performed.
Based on the findings in this study, it is concluded that additional antennas add a significant gain in throughput, specifically by obtaining additional diversity from STBC in the low SNR regime and SMUX in the high SNR regime.

Preface

This report is written as a part of a master thesis in the specialization Software Defined Radios at Aalborg University. The work has been carried out in collaboration with Intel, Aalborg, which kindly offered desk, lunch, and equipment for unlimited use during my work on this thesis.

The work for this thesis has been conducted under supervision from Gert Frølund Pedersen, AAU, who put a great effort into guiding me towards a successful thesis. Furthermore, a special thank to Christian Rom, IMC, who has used an endless amount of hours discussing, explaining and introducing me to the theories of the unequalled MIMO world. Also, thanks to Tommaso Balercia, IMC for the help with geometric MIMO channel models and for reviewing the report, to Xavier Carreno, IMC for the valuable, although sometimes painful, discussions we had and to Michael Knudsen, IMC for putting me into the right track from the beginning. Last but not least, thanks to my girlfriend, Anne Sig Vestergaard fordi du kunne leve med at jeg, aften efter aften, kom hjem kun for at sove og tage afsted igen.

Included in this report is a CD, on which an electronic version of this report, together with the simulator developed during this project can be found.

Troels Jessen

Chapter 1

Reading guide

In **chapter 3**, an exhaustive survey of SISO, SIMO and MIMO algorithms are presented and analyzed. The chapter has Appendix A, BER derivations associated for further analysis of theoretical BER derivations.

Chapter 4 takes the receive chain a step further by describing soft demodulation, Turbo coding, and rate matching to present plots of throughput, which complies with LTE expected performance.

Chapter 4 presents more sophisticated channel models, these evolving from statistical as well as geometrical properties. Furthermore, a geometrical channel model usable for specific investigation in the angular domain, when using MIMO, is developed.

In all chapters, simulations are shown to support the theoretical descriptions and derivations. Because of figures and illustrations, the report is best viewed in color, and should not be printed in B/W.

1.1 Symbols

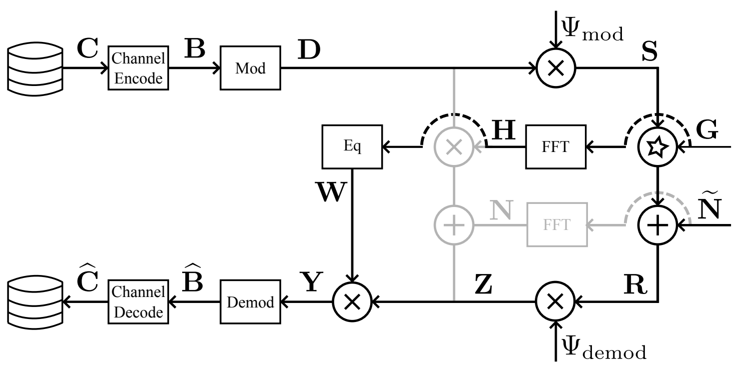

Figure 1.1: System model with notation as used in this report

1.2 Abbreviations

AoA Angle of Arrival

AoD Angle of Departure

BER Bit Error Rate

BCJR Bahl-Cocke-Jelinek-Raviv

CN Condtion Number

CP Cyclic Prefix

CSI Channel State Information

DCN Demmel Condition Number

FEC Forward Error Correcting

ICI Inter Carrier Interference

i.i.d. Independent and Identically Distributed

ISI Inter-Symbol Interference

IST Information Society Technologies

LLR Log-likelihood Ratio

MRC Maximum-Ratio Combining

MSE Mean Square Error

MMSE Minimum Mean Square Estimater

NLOS Non-Line Of Sight

OSIC Ordered Successive Interference Cancellation

PDF Probability Density Function

PSK Phase Shift Keying

QAM Quadrature Amplitude Modulation

QPP Quadratic Permutation Polynomial

SER Symbol Error Rate

SIC Successive Interference Cancellation

STBC Space-Time Block Codes

SMUX Spatial Multiplexing

WINNER Wireless World Initiative New Radio

ZF Zero Forcing

Contents

Chapter 2

Introduction

2.1 History of wireless digital communication

During the last centuries, the technology behind wireless communication has developed at a dramatical rate; from analogously transmitted signals to channel adaptive, multi-antenna digital systems. Since the eighteenth century scientists have believed in a relationship between electricity and magnetism. In 1820, the famous Danish physicist Hans Christian Ørsted observed that a compass needle was affected by the current in a nearby electrical wire; a phenomenon that André-Marie Ampère shortly after presented a paper about. In 1861, James Clerk Maxwell presented what would later be known as Maxwell's equations that, among other things, define the four laws about electromagnetism[1]. Maxwell's equations, rewritten by Heaviside, formed the reason for the development of the first wireless transmitters and receivers. In the late 1880s, Heinrich Hertz managed to prove the prediction of Maxwell's equations by creating an antenna system. By that antenna system, he managed to transmit the first electromagnetic signal over short distance and even to demonstrate the diffraction and reflection properties of wireless signals.

Hertz did, however, not realize the potential of his invention and the world had to wait until 1892, in which year Nikola Tesla stated that the technology could be used to transmit signals from one place to another.

A few years later, Oliver Lodge managed to transmit a Morse code 150 m through a wireless environment, which made him the first person to show the usefulness of wireless transmission. He furthermore showed that the system could be radically improved by using a receiver that was tuned to the specific frequency of the transmitter. One year later, Guglielmo Marconi demonstrated a wireless transmission over 1.5 km. The British Post Office showed interest in the invention as an alternative to the expensive wired telegraphy lines, especially across the Atlantic Ocean. In 1901, Marconi managed to do the first transatlantic transmission by transmitting the letter "s" from England to Canada, although critics claimed that Marconi had received only noise and that the decoding was pure luck. Nevertheless, Marconi in 1907 established a radio and telegraph service, providing transmission services across the

Atlantic Ocean. Marconi also supplied the wireless technology on the RMS Titanic, which is said to be the reason for every man which was saved during the catastrophic incident.

Shortly after, World War I created a demand of the new technologies. The Royal Flying Corps of England, founded in 1912 with Major Herbert Musgrave being the head of the research section, developed a wireless transmitter, which was used from the beginning of the war in 1914. This transmitter allowed observers in aircrafts to transmit locations of enemy targets to the artillery commander on the ground. In 1916, a new lightweight receiver was developed to be carried on aircrafts, enabling the British to create a better defense against the German bomb raids. The system required the unreeling of a 50 m antenna from the plane before its use[2].

The problem of the initial transmitters was that the transmissions consisted of short pulses with a huge frequency spread, even though simple filters were fitted to the antenna circuits. Soon after World War I, Edwin Armstrong began working on continuous-wave transmissions that modulated Morse codes on the carrier frequency and a frequency that was slightly higher, thereby defining the Frequency-shift keying transmission[3]. In the same years, vacuum tubes and later transistors made it possible to use higher carrier frequencies.

In 1926, John B. Johnson managed to measure thermal background noise that exist in all electrical equipment[4]. This noise influences all basic wireless communication, and is an important concern in all wireless communication systems.

In the 1930s, engineers discovered the opportunities hidden in using short waves (wavelengths of 15 to 60 m) and observed problems as fading and echoes. Soon after, the first suggestions appeared that multiple receive antennas could be used to gain diversity of the signals.

Soon after World War II, mobile telephony was made public, with the first interconnection between mobile and wired telephones done in 1946. Since then, the extent of wireless telephony has increased dramatically, especially with the GSM[1] defined in 1989 as the first digital cell phone network being deployed in the following years. The GSM network was extended with GPRS[2] to supply users with a packet-based network. The system evolved into EDGE[3], the first cellular system to use phase modulated signals, which were relevant in order to pack more information on a given frequency band, since the frequency spectrum was getting crowded as wireless usage got more common. Meanwhile, the well-known 802.11 WLAN evolved in speed and technologies, from plain PSK[4] with DSSS[5] to using OFDM[6] to increase throughput.

Since Gerard J. Foschini presented BLAST[7] in 1996, spatial multiplexing is

[1] Groupe Spècial Mobile
[2] General Packet Radio Services
[3] Enhanced Data rates for GSM Evolution
[4] Phase-shift Keying
[5] Direct Sequence Spread Spectrum
[6] Orthogonal Frequency Division Multiplexing
[7] Bell Laboratories Layered Space-Time

recognized as a possibility to gain throughput in a communication system with multi-antennas at transmitter and receiver. The latest newcomer in mobile communication is LTE[8], which uses an adaptive QAM[9] modulation encapsulated in OFDM and spatial multiplexing when applicable.

2.2 Problem statement

Adding more antennas to the communication system is the latest trend in wireless communication. A lot of investigation is yet to be done, though. As a result, this project focuses on answering the following question:

> ***How can multiple antennas affect the quality and throughput of a wireless channel?***

And in particular investigating

- Receiver structures for MIMO[10] systems
- Channel models capable of simulating MIMO
- Channel properties affecting MIMO capabilities

2.2.1 Scope and limitations

In this thesis, the focus will be on receiver structures in varying MIMO channel conditions. Channel estimation will not be investigated. Perfect channel knowledge is expected to be available on the receiver side, while no channel knowledge will be available to the transmitter.

---

[8] Long Term Evolution

[9] Quadrature Amplitude Modulation

[10] Multipe Input Multiple Output

Chapter 3

Receiver algorithms

The mobile wireless channel is dynamic, difficult to predict, and ever changing. Therefore, mathematical models have been defined to permit simulations without performing costly experiments in the real environment. In this chapter, a statistical channel model and different receiver algorithms are defined and analyzed by simulating the achieved BER[1].

3.1 AWGN channel

A wireless transmission in its simplest form is defined as

$$z = d + n \tag{3.1}$$

$$\hat{d} = \text{desc}\langle y \rangle \tag{3.2}$$

$$n = \mathcal{N}\left(0, \frac{N_0}{2}\right) + \mathcal{N}\left(0, \frac{N_0}{2}\right) j \tag{3.3}$$

where

- d is the transmitted symbol
- n is a complex gaussian uncorrelated sequence
- z is the received symbol
- $\text{desc}\langle\cdot\rangle$ is the hard decision rule
- $\hat{d}$ is the received symbol, derived by a hard decision rule

In this report, only M-PSK[2] and M-QAM[3] signals will be considered. In these cases, the symbols can be defined as complex numbers, representing the baseband amplitude and phase of the given symbol.

[1] Bit Error Rate
[2] Phase Shift Keying
[3] Quadrature Amplitude Modulation

3.1.1 Verification of BER in AWGN channel

In appendix A.1, the theoretical SER[4] and BER for M-PSK in an AWGN channel is derived as

$$P_{b,\mathrm{BPSK}} = Q\left(\sqrt{\frac{2\mathcal{E}_s}{N_0}}\right) \tag{3.4}$$

and

$$P_{b,\mathrm{QPSK}} = Q\left(\sqrt{\frac{\mathcal{E}_s}{N_0}}\right) \tag{3.5}$$

respectively, with $\mathcal{E}_s$ being the energy per symbol. Figure 3.1 shows a comparison of BER in BPSK, QPSK, 16-QAM and 64-QAM symbol constallations in an AWGN channel. The theoretical BER for 16-QAM and 64-QAM is shown in appendix A.1.3.

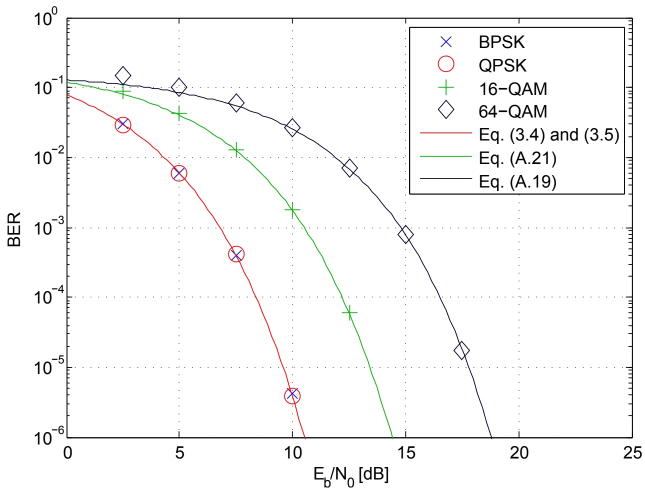

Figure 3.1: BER versus $\mathcal{E}_b/N_0$ of various phase modulated constellations in an AWGN channel.

Figure 3.1 illustrates the BER with respect to $\mathcal{E}_b/N_0$. This plot can be used to compare the BER of different modulation orders when a certain amount of energy is used to transfer each bit. As the theoretical derivation in appendix A.1 showed, the BER for BPSK and grey coded QPSK are equal. Notice that the approximation in equation (A.21) for M-QAM BER holds in the high SNR regime, while the simulated BER is higher than the theoretical analogue in the low SNR regime (above 10^{-2}), because of the possibility that more than one bit per symbol will be wrongly decoded.

3.2 Rayleigh fading channel

When a signal propagates through a typical physical environment, it travels through different paths as in figure 3.2, creating the risk of destructive interference (figure 3.3). Additionally, if one or both terminals are moving or if

[4] Symbol Error Rate

the environment is changing, the channel properties will vary dynamically over time and thereby create a demand for monitoring the channel continuously.

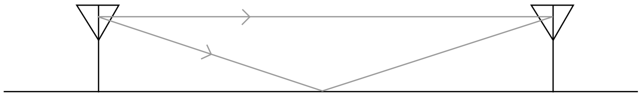

Figure 3.2: Multipath propagation channel.

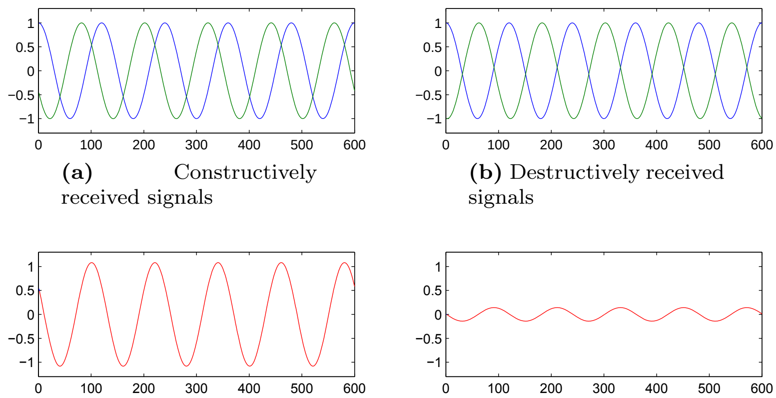

(a) Constructively received signals

(b) Destructively received signals

(c) Result of constructively received signals

(d) Result of destructively received signals

Figure 3.3: In (a) and (c) a set of constructively received signals and the resultant signal are shown. In (b) and (d) the consequences of destructively received signals are shown.

If the phase and amplitude of the received signals are i.i.d.[5] vectors without a dominating component and there is a significant number of contributions, the resultant signal amplitude has a Rayleigh distribution[5, sec. 13.1-2]. In this case, the received signal is defined as

$$z = \alpha e^{j\phi} d + n \tag{3.6}$$

where

- α is a Rayleigh distributed amplitude,
- $e^{j\phi}$ is a uniformly distributed phase in range $[-\pi, \pi]$.

[5]Independent and Identically Distributed

3.2.1 Verification of BER in Rayleigh channel

In appendix A.2, the theoretical BER for M-PSK signals in Rayleigh fading are derived as

$$P_{b,\mathrm{BPSK}} = \frac{1}{2}\left(1 - \sqrt{\frac{\bar{\gamma_s}}{1+\bar{\gamma_s}}}\right) \tag{3.7}$$

and

$$P_{b,\mathrm{QPSK}} = \frac{1}{2}\left(1 - \sqrt{\frac{\bar{\gamma_s}}{2+\bar{\gamma_s}}}\right) \tag{3.8}$$

with

$$\bar{\gamma_s} = \frac{\mathcal{E}_s}{N_0}\mathrm{E}\left[\alpha^2\right] \tag{3.9}$$

where α is the Rayleigh distributed instantaneous channel gain. In figure 3.4, the simulated BER for BPSK, QPSK, 16-QAM and 64-QAM. It is seen that the slope of the lines for the different modulation schemes are equal, while the power gain of the modulation schemes is changed.

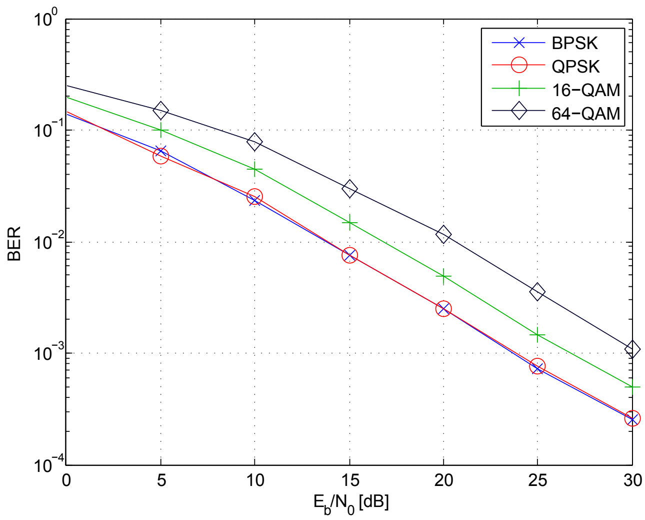

Figure 3.4: BER of various phase modulated modulation forms in a Rayleigh fading channel with respect to $\mathcal{E}_b/N_0$.

If figure 3.4 is compared with the figure of AWGN BER in section 3.1.1, it is clear that the performance is heavily degraded in a fading environment. This is the motivation for the following sections, which will focus on how to deal with and counteract the effects of fading.

3.3 Multipath propagation

From the previous sections it is clear that the multipath effect has a negative impact on the received signal. Apart from the cancellation effect observed in figure 3.3, multipath also causes ISI[6] when the delay spread is significant compared to the symbol time. To counteract ISI, modern communication systems utilize OFDM, which is described in appendix B. OFDM allows to reduce the symbol time and possibly add CP[7], which makes it possible to eliminate ISI.

Methods have been developed to measure this multipath effect, the outcome of which is a channel impulse response $\mathbf{g}$, describing the channel responses in the time domain.

The multipath propagation can be effectivly represented from the CIR $\mathbf{g}$ that characterizes a given channel. That is

$$\mathbf{z} = \mathbf{g} \star \mathbf{s} + \mathbf{n} \tag{3.10}$$

with $\mathbf{s}$ being the time-domain OFDM symbol. $\mathbf{g}$ is considered to be constant throughout one OFDM symbol time. Delayed versions of the symbols caused by the multipath effect are added to the next OFDM symbols. The effect is graphically shown in figure 3.5.

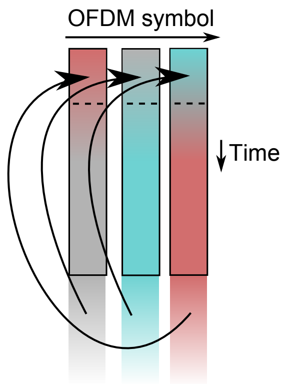

Figure 3.5: The convolution of a block of OFDM symbols; the part above the dashed line symbolizes the CP. It is shown how multipath has effect on the next symbol in the block. When the channel impact propagates besides the CP, the OFDM signal quality will degrade because of ISI. To emulate an infinite size OFDM symbol in the simulations, the last multipath effect is added to the beginning of the first OFDM symbol.

Due to the type of relation between the time and frequency domain, the channel transfer function $\mathbf{h} = \mathrm{DFT}(\mathbf{g})$ will be more coarse if the delay spread increases. But as each subcarrier is relatively narrow in frequency, the channel can be expected to be frequency flat for one OFDM symbol.

[6]Inter-Symbol Interference
[7]Cyclic Prefix

3.3.1 BER in multipath Rayleigh environment

From section A.2 it is known that the average SNR in a Rayleigh fading environment is

$$\overline{\gamma} = \frac{\mathcal{E}_s}{N_0} \mathrm{E}\left[\alpha^2\right]. \tag{3.11}$$

When the signal undergoes multipath propagation, this equation is extended to

$$\overline{\gamma} = \frac{\mathcal{E}_s}{N_0} \mathrm{E}\left[\sum_k |h_k|^2\right] \tag{3.12}$$

because the power of all delay tabs can be combined during the equalization in the receiver. To calculate the error rate from $\overline{\gamma}$, the equations derived from Rayleigh fading error rates in section A.2 can be utilized with α^2 being the total energy of the channel.

3.4 Receive diversity

From section 3.2.1 it is clear that fading heavily degrades the performance of communication channels. Diversity is a method often used to counteract the effects of fading. Diversity can be intended in space, time, or frequency. A popular method is to introduce additional antennas at the receiver, making the received signal

$$\mathbf{z} = \mathbf{h}d + \mathbf{n}. \tag{3.13}$$

If the elements in the receiver array are placed with sufficient distance between each other, the influence of the channel on the received signal can be considered uncorrelated in space. Going from the worst to the best, the transmitted symbol can be derived from the received symbols using[6]:

- **Switched Combining:** This scheme monitors the SNR of the currently used receive antenna element. When this drops lower than a predefined value, the receiver switches and receives from another antenna.
- **Selection Combining:** This scheme monitors the SNR of all antennas, and uses the one with the highest gain.
- **Equal Gain Combining:** This scheme uses a mean of all phase-corrected received signals.
- **Maximal-Ratio Combining:** This scheme uses all received signals, normalized in proportion to the SNR of the different receive antennas to recreate the transmitted symbol. In the following, only MRC[8] will be considered. A basic structure of a MRC receiver is shown in figure 3.6.

[8] Maximum-Ratio Combining

3.4.1 Derivation of MRC

If no interference is present, the optimal linear solution for receive combining is the MRC, as it optimizes the SNR of the received symbol[7]. In this section, an MRC equalizer will be derived.

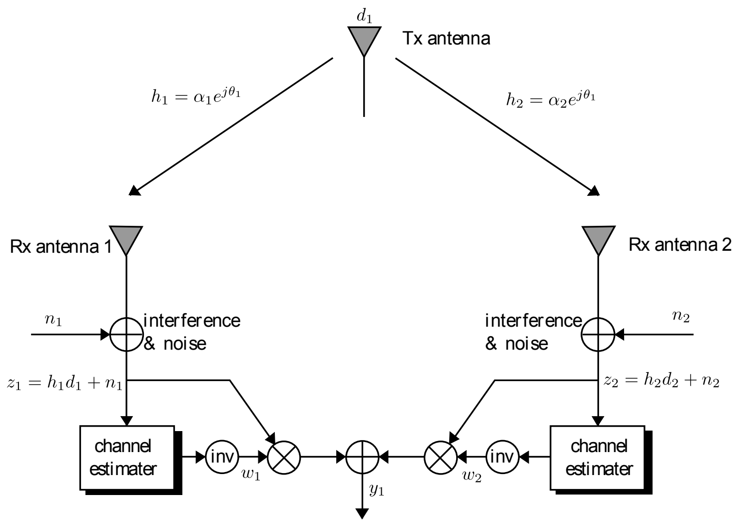

Figure 3.6: Structural SIMO receiver. Created with inspiration from [8].

The SNR on the r'th receive antenna before the equalization is defined as

$$SNR_r = |h_r|^2 \frac{\sigma_d^2}{\sigma_n^2} \tag{3.14}$$

with $\sigma_d^2 = \mathrm{E}\left[d_r^2\right]$ being the average energy per bit and $\sigma_n^2 = \mathrm{E}\left[n_r^2\right]$ being the expected noise energy of any receive antenna. Since the received symbol is equalized as $y = \mathbf{wz} = \mathbf{w}(\mathbf{h}d + \mathbf{n}) = \mathbf{wh}d + \mathbf{wn}$, the SNR of the equalized symbol is

$$SNR = \frac{\mathrm{E}\left[|\mathbf{wh}d|^2\right]}{\mathrm{E}\left[|\mathbf{wn}|^2\right]} = \frac{|\sum_r w_r h_r|^2 \,\mathrm{E}\left[|d|^2\right]}{|\sum_r w_r|^2 \,\mathrm{E}\left[|n_r|^2\right]} \tag{3.15}$$

with $\mathbf{w}$ being a $N_{\mathrm{Rx}} \times 1$ vector, which optimizes the SNR of the received symbol.

Due to the fact that $\mathbf{wh}$ is independent of $\mathrm{E}\left[|d|^2\right]$ and $\mathbf{w}$ is independent of $\mathrm{E}\left[|d|^2\right]$, equation (3.15) can be simplified into

$$SNR = \frac{\sigma_d^2 \,|\sum_r w_r h_r|^2}{\sigma_n^2 \,|\sum_r w_r|^2}. \tag{3.16}$$

To derive $\mathbf{w}$, the Cauchy-Schwarz inequality

$$\left|\sum_i x_i y_i\right|^2 \leq \left(\sum_j |x_j|^2\right)\left(\sum_k |y_k|^2\right) \tag{3.17}$$

is utilized. If $c\mathbf{x}^{\mathrm{H}} = \mathbf{y}$, with c being some scalar component, eq. (3.17) is an equality. To utilize the inequality, $\mathbf{x}$ and $\mathbf{y}$ are defined

$$x_j = w_j \frac{\sigma_n}{\sigma_d} \tag{3.18}$$

$$y_k = h_k \frac{\sigma_d}{\sigma_n} \tag{3.19}$$

so that

$$\left| \sum_i w_i \frac{\sigma_n}{\sigma_d} h_i \frac{\sigma_d}{\sigma_n} \right|^2 \leq \left(\sum_j \left| w_j \frac{\sigma_n}{\sigma_d} \right|^2 \right) \left(\sum_k \left| h_k \frac{\sigma_d}{\sigma_n} \right|^2 \right), \tag{3.20}$$

which is equivalent to writing

$$\left| \sum_i w_i h_i \right|^2 \leq \left(\sum_j \left| w_j \frac{\sigma_n}{\sigma_d} \right|^2 \right) \left(\sum_k \left| h_k \frac{\sigma_d}{\sigma_n} \right|^2 \right). \tag{3.21}$$

The inequality in eq. (3.21) can now be rearranged to reflect the SNR definitions in eq. (3.16) and eq. (3.14):

$$SNR = \frac{\left|\sum_i w_i h_i\right|^2}{\sum_j \left| w_j \frac{\sigma_n}{\sigma_d} \right|^2} \leq \sum_k \left| h_k \frac{\sigma_d}{\sigma_n} \right|^2 = \sum_r SNR_r \tag{3.22}$$

$$\tag{3.23}$$

from which

$$SNR = \frac{\left|\sum_i w_i h_i\right|^2 \sigma_d^2}{\sum_j |w_j|^2 \sigma_n^2} \leq \sum_k |h_k|^2 \frac{\sigma_d^2}{\sigma_n^2} = \sum_r SNR_r. \tag{3.24}$$

appears. Interestingly, eq. (3.24) shows that the best possible SNR is obtained when $\mathbf{w} = c\mathbf{h}^{\mathrm{H}}$ and that, in this case, the SNR of the equalized symbol y equals the sum of the SNR's of the received symbols $\mathbf{x}$. This means that

$$y_{\text{phase}} = c\mathbf{h}^{\mathrm{H}}\mathbf{z} = c\mathbf{h}^{\mathrm{H}}\mathbf{h}d + c\mathbf{h}^{\mathrm{H}}\mathbf{n}. \tag{3.25}$$

If M-QAM is used, c must be chosen so that the amplitude of the transmitted symbol is restored. Therefore, c can be chosen so that

$$\mathbf{w} = \frac{\mathbf{h}^{\mathrm{H}}}{\mathbf{h}^{\mathrm{H}}\mathbf{h}}. \tag{3.26}$$

This allows to compensate for the impact that the channel has on the amplitude. When implemented, the received symbol equalized by a MRC is thus

$$y = \mathbf{w}\mathbf{z} = \frac{\mathbf{h}^{\mathrm{H}}}{\mathbf{h}^{\mathrm{H}}\mathbf{h}}\mathbf{z} = d + \frac{\mathbf{h}^{\mathrm{H}}}{\mathbf{h}^{\mathrm{H}}\mathbf{h}}\mathbf{n}. \tag{3.27}$$

3.4.2 Verification of receive diversity

In figure 3.7 a simulation of the BER for different numbers of antenna elements is seen. It is clear that adding multiple antennas results in a significant BER improvement. The simulation is done in an uncorrelated Rayleigh fading channel using 16-QAM and an MRC equalizer for diversity combining. The result matches those illustrated in [9].

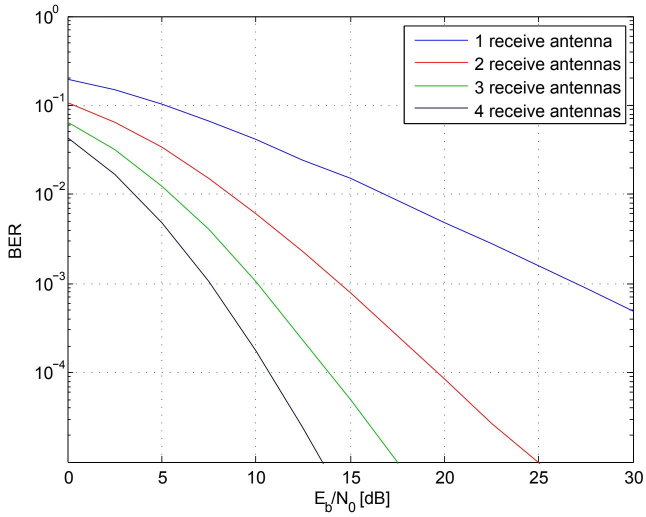

Figure 3.7: BER of 16-QAM signal with multiple receive antennas configured for diversity with MRC.

3.5 Space-Time transmit diversity

Equipping a system with a large number of antennas is typically an expensive and complicated process. It is thus important to have a method that can always exploit the diversity offered by the additional antennas. In 1998, Alamouti [8] suggested the use of STBC[9] which, by resorting to two transmit antennas or at two separate frequencies in a wideband channel, allowed simultaneous transmission of two symbols over two symbol times to achieve diversity gain. According to the method, the symbols are transmitted as

$$\begin{bmatrix} z_1 & z_2 \end{bmatrix} = \begin{bmatrix} h_1 & h_2 \end{bmatrix} \begin{bmatrix} d_1 & d_2 \\ -d_2^* & d_1^* \end{bmatrix} + \begin{bmatrix} n_1 & n_2 \end{bmatrix} \tag{3.28}$$

with d_1, d_2 being transmitted in the first symbol time, and $-d_2^*, d_1^*$ transmitted in the second symbol time. The channel must remain constant during two time slots for the method to be applicable. From equation (3.28), y_1 and y_2 can be derived at the receiver as

$$z_1 = h_1 d_1 + h_2 d_2 + n_1 \tag{3.29}$$

$$z_2 = -h_1 d_2^* + h_2 d_1^* + n_2 \tag{3.30}$$

$$\downarrow$$

$$z_2^* = h_2 d_1 - h_1 d_2 + n_2^* \tag{3.31}$$

which in turn can be written in matrix form as

$$\begin{bmatrix} z_1 \\ z_2^* \end{bmatrix} = \begin{bmatrix} h_1 & h_2 \\ h_2^* & -h_1^* \end{bmatrix} \begin{bmatrix} d_1 \\ d_2 \end{bmatrix} + \begin{bmatrix} n_1 \\ n_2^* \end{bmatrix}. \tag{3.32}$$

[9]Space-Time Block Codes

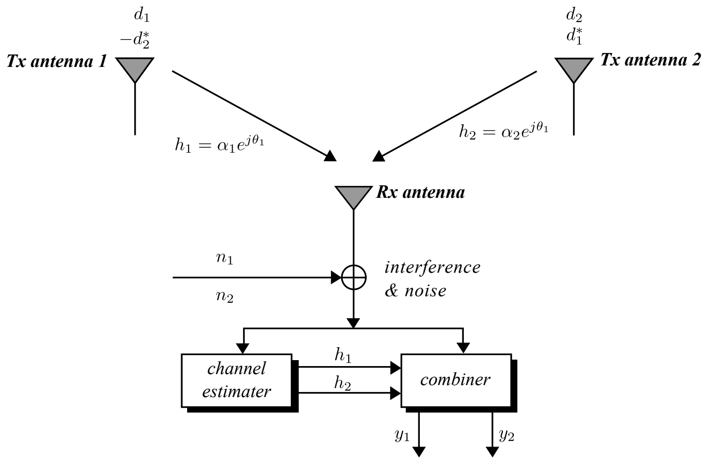

Figure 3.8: Structural MISO receiver with Alamouti coding. The first lines indicate the transmitted symbol for time 1, the second line indicates the symbol transmitted for symbol time 2. Figure created with inspiration from [8].

The received symbols y_1 and y_2 are calculated as

$$\begin{bmatrix} y_1 \\ y_2 \end{bmatrix} = \begin{bmatrix} h_1 & h_2 \\ h_2^* & -h_1^* \end{bmatrix}^{-1} \left(\begin{bmatrix} z_1 \\ z_2^* \end{bmatrix} \right) \tag{3.33}$$

$$= \frac{1}{|h_1|^2 + |h_2|^2} \begin{bmatrix} h_1^* & h_2 \\ h_2^* & -h_1 \end{bmatrix} \left(\begin{bmatrix} d_1 \\ d_2^* \end{bmatrix} + \begin{bmatrix} n_1 \\ n_2^* \end{bmatrix} \right). \tag{3.34}$$

Equation (3.34) shows that, since the noise is uncorrelated, the two symbols can be derived as

$$y_1 = \frac{h_1^* z_1 + h_2 z_2^*}{|h_1|^2 + |h_2|^2} \tag{3.35}$$

$$y_2 = \frac{h_2^* z_1 - h_1 z_2^*}{|h_1|^2 + |h_2|^2} \tag{3.36}$$

As an additional note, it should be observed that if the amplitude of the symbol is irrelevant for the demodulation (M-PSK), the scaling of the channel matrix can be omitted, leaving only a matrix, which appears to be the Hermitian transpose of the channel matrix in eq. (3.32). This enables a simple structure in the receiver.

3.5.1 STBC with multiple receive antennas

As an introduction to spatial multiplexing, the method presented in section 3.5 will be taken one step further by considering multiple receive antennas to achieve additional diversity.

For a system like the one in figure 3.9, the received signal is defined as

$$\begin{bmatrix} \mathbf{z_1} & \mathbf{z_2} \end{bmatrix} = \begin{bmatrix} \mathbf{h_1} & \mathbf{h_2} \end{bmatrix} \begin{bmatrix} d_1 & -d_2^* \\ d_2 & d_1^* \end{bmatrix} + \begin{bmatrix} \mathbf{n_1} & \mathbf{n_2} \end{bmatrix} \tag{3.37}$$

with $\mathbf{z_1}$, $\mathbf{z_2}$, $\mathbf{h_1}$, $\mathbf{h_2}$, $\mathbf{n_1}$, $\mathbf{n_2}$ being vectors of size equal to the number of receive antennas.

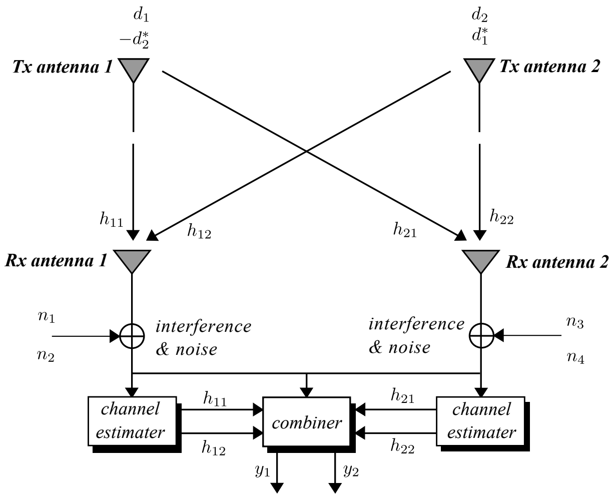

Figure 3.9: Structural MIMO receiver with Alamouti coding. Created with inspiration from [8].

For a case with two receive antennas, the received symbols are derived as

$$\begin{bmatrix} z_{11} & z_{12} \\ z_{21} & z_{22} \end{bmatrix} = \begin{bmatrix} h_{11} & h_{12} \\ h_{21} & h_{22} \end{bmatrix} \begin{bmatrix} d_1 & -d_2^* \\ d_2 & d_1^* \end{bmatrix} + \begin{bmatrix} n_{11} & n_{12} \\ n_{21} & n_{22} \end{bmatrix} \tag{3.38}$$

which can be rearranged as

$$\begin{bmatrix} z_{11} \\ z_{12}^* \\ z_{21} \\ z_{22}^* \end{bmatrix} = \begin{bmatrix} h_{11} & h_{12} \\ h_{12}^* & -h_{11}^* \\ h_{21} & h_{22} \\ h_{22}^* & -h_{21}^* \end{bmatrix} \begin{bmatrix} d_1 \\ d_2 \end{bmatrix} + \begin{bmatrix} n_{11} \\ n_{12}^* \\ n_{21} \\ n_{22}^* \end{bmatrix}. \tag{3.39}$$

Inverting according to the Moore-Penrose pseudo-inverse[5, eq. (A-27)], i.e. calculating

$$\mathbf{W} = \mathbf{H}^\dagger = \left(\mathbf{H}^{\mathrm{H}}\mathbf{H}\right)^{-1}\mathbf{H}^{\mathrm{H}}, \tag{3.40}$$

the received symbols can thus be written as

$$\begin{bmatrix} y_1 \\ y_2 \end{bmatrix} = \frac{\begin{bmatrix} h_{11}^* & h_{12} & h_{21}^* & h_{22} \\ h_{12}^* & -h_{11} & h_{22}^* & -h_{21} \end{bmatrix}}{|h_{11}|^2 + |h_{21}|^2 + |h_{12}|^2 + |h_{22}|^2} \left(\begin{bmatrix} z_{11} \\ z_{12} \\ z_{21} \\ z_{22} \end{bmatrix} + \begin{bmatrix} n_{11} \\ n_{12}^* \\ n_{21} \\ n_{22}^* \end{bmatrix} \right). \tag{3.41}$$

3.5.2 Verification of transmit diversity

Figure 3.10 shows the error probabilities with different number of elements at the transmitter and the receiver. The simulation is conducted in an uncorrelated Rayleigh fading channel using 16-QAM. For comparison, the BER for receive diversity derived in section A.3 is shown. From this, it is seen that using multiple antennas at the receiver adds the same diversity gain, but also an additional power gain compared to transmit diversity. The reason for this is that the energy per antenna with transmit diversity is halved to keep the $\mathcal{E}_b/N_0$.

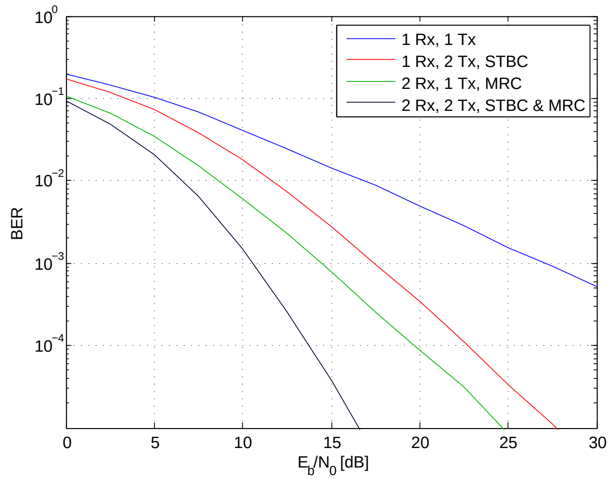

Figure 3.10: BER of 16-QAM signal with multiple transmit and receive antennas configured for diversity with Alamouti coding scheme and MRC.

3.6 Spatial multiplexing

If the system contains multiple transmit and receive antenna elements and the channel is sufficiently uncorrelated, it is possible to transmit multiple symbols during each symbol time. The following sections derive methods for channel equalization and detection in a MIMO multiplexing system. Again, the channel is assumed to be narrowband and not to change during one symbol time.

The received symbol vector in a MIMO system is

$$\mathbf{z} = \mathbf{H}\mathbf{d} + \mathbf{n} \tag{3.42}$$

with $\mathbf{d}$ having dimensions $N_{\mathrm{Tx}} \times 1$ and $\mathbf{H}$ having dimensions $N_{\mathrm{Rx}} \times N_{\mathrm{Tx}}$.

3.6.1 Zero Forcing equalization

The obvious way of deriving the estimated symbols $\mathbf{y}$ is to multiply the received symbol vector with an inverted channel matrix. This method is known as ZF[10] and is optimal with respect to nulling out the interfering signals. Unfortunately, however, it has a tendency to enhance noise. Since the number of transmit and receive antennas are not necessarily equal, the inversion can be done using the Moore-Penrose pseudo-inverse, i.e. by posing

$$\mathbf{W} = \left(\mathbf{H}^{\mathrm{H}}\mathbf{H}\right)^{-1}\mathbf{H}^{\mathrm{H}}, \tag{3.43}$$

which implies

$$\mathbf{y} = \mathbf{W}\mathbf{z} \tag{3.44}$$

3.6.1.1 Derivation of Zero Forcing

In order to illustrate the influence of ZF, the attention will be focused on a 2×2 system.

The received symbols can be written as

$$\begin{bmatrix} z_1 \\ z_2 \end{bmatrix} = \begin{bmatrix} h_{11} & h_{12} \\ h_{21} & h_{22} \end{bmatrix} \cdot \begin{bmatrix} d_1 \\ d_2 \end{bmatrix} + \begin{bmatrix} n_1 \\ n_2 \end{bmatrix}. \tag{3.45}$$

Because $\mathbf{H}$ in (3.45) is a $N \times N$ matrix, the received symbols can be derived from the direct matrix inversion as

$$\begin{bmatrix} y_1 \\ y_2 \end{bmatrix} = \frac{1}{h_{11}h_{22} - h_{12}h_{21}} \begin{bmatrix} h_{22} & -h_{12} \\ -h_{21} & h_{11} \end{bmatrix} \cdot \begin{bmatrix} h_{11}d_1 + h_{12}d_2 + n_1 \\ h_{21}d_1 + h_{22}d_2 + n_2 \end{bmatrix} \tag{3.46}$$

Building on eq. (3.46), y_1 can be written as

$$\begin{aligned} y_1 &= \frac{h_{22}\left(h_{11}d_1 + h_{12}d_2 + n_1\right) - h_{12}\left(h_{21}d_1 + h_{22}d_2 + n_2\right)}{h_{11}h_{22} - h_{12}h_{21}} \\ &= \frac{d_1\left(h_{11}h_{22} - h_{12}h_{21}\right) + h_{22}n_1 - h_{12}n_2}{h_{11}h_{22} - h_{12}h_{21}} \\ &= d_1 + \frac{h_{22}n_1 - h_{12}n_2}{h_{11}h_{22} - h_{12}h_{21}}. \end{aligned} \tag{3.47}$$

Equation (3.47) shows that the interfering signals are nulled out completely, making the equalizer optimal in a noiseless environment. Nevertheless, because of the inversion, the equalizer might amplify the noise if some channel coefficients are low. This effect makes the equalizer sensible to noise and therefore not suitable for use in noisy environments.

---

[10] Zero Forcing

3.6.2 Minimum Mean Square Estimator

Instead of inverting the matrix, it is possible to use a statistical approach. The vector error of an equalized symbol is $\mathbf{d}-\mathbf{W}\mathbf{z}$, so the MSE[11] becomes

$$\epsilon^2 = \mathrm{E}\left[|\mathbf{d}-\mathbf{W}\mathbf{z}|^2\right]. \tag{3.48}$$

To minimize this expression, its derivative must be calculated and set equal to zero. To do that, the equation must be rearranged as

$$\begin{aligned}\epsilon^2 &= \mathrm{E}\left[\left((\mathbf{d}-\mathbf{W}\mathbf{z})^{\mathrm{H}}(\mathbf{d}-\mathbf{W}\mathbf{z})\right)\right]\\ &= \mathrm{E}\left[\mathrm{tr}\left((\mathbf{d}-\mathbf{W}\mathbf{z})\left(\mathbf{d}^{\mathrm{H}}-\mathbf{z}^{\mathrm{H}}\mathbf{W}^{\mathrm{H}}\right)\right)\right]\\ &= \mathrm{E}\left[\mathrm{tr}\left(\mathbf{d}\mathbf{d}^{\mathrm{H}}-\mathbf{d}\mathbf{z}^{\mathrm{H}}\mathbf{W}^{\mathrm{H}}-\mathbf{W}\mathbf{z}\mathbf{d}^{\mathrm{H}}+\mathbf{W}\mathbf{z}\mathbf{z}^{\mathrm{H}}\mathbf{W}^{\mathrm{H}}\right)\right]\end{aligned} \tag{3.49}$$

with $\mathrm{tr}(\mathbf{X})=\sum_i \mathbf{X}_{ii}$, $\mathbf{x}^{\mathrm{H}}\mathbf{x}=\mathrm{tr}\left(\mathbf{x}\mathbf{x}^{\mathrm{H}}\right)$ and $(\mathbf{A}\mathbf{B})^{\mathrm{H}}=\mathbf{B}^{\mathrm{H}}\mathbf{A}^{\mathrm{H}}$. By remembering that

$$\frac{\mathrm{d}}{\mathrm{d}\mathbf{X}}\mathrm{tr}(\mathbf{X}\mathbf{A}) = \mathbf{A}^{\mathrm{H}}, \tag{3.50}$$

$$\frac{\mathrm{d}}{\mathrm{d}\mathbf{X}}\mathrm{tr}\left(\mathbf{A}\mathbf{X}^{\mathrm{H}}\right) = \mathbf{A}^{\mathrm{H}}, \tag{3.51}$$

$$\frac{\mathrm{d}}{\mathrm{d}\mathbf{X}}\mathrm{tr}\left(\mathbf{X}\mathbf{A}\mathbf{X}^{\mathrm{H}}\right) = \mathbf{X}\mathbf{A}^{\mathrm{H}}+\mathbf{X}\mathbf{A}, \tag{3.52}$$

the derivative with respect to $\mathbf{W}$ can be expressed as

$$\begin{aligned}\frac{\mathrm{d}}{\mathrm{d}\mathbf{W}}\epsilon^2 &= \mathrm{E}\left[-\left(\mathbf{d}\mathbf{z}^{\mathrm{H}}\right)^{\mathrm{H}}-\mathbf{z}\mathbf{d}^{\mathrm{H}}+\mathbf{W}\left(\mathbf{z}\mathbf{z}^{\mathrm{H}}\right)^{\mathrm{H}}+\mathbf{W}\mathbf{z}\mathbf{z}^{\mathrm{H}}\right]\\ &= \mathrm{E}\left[-2\mathbf{z}\mathbf{d}^{\mathrm{H}}+2\mathbf{W}\mathbf{z}\mathbf{z}^{\mathrm{H}}\right]\\ &= \mathrm{E}\left[-2(\mathbf{H}\mathbf{d}+\mathbf{n})\mathbf{d}^{\mathrm{H}}+2\mathbf{W}(\mathbf{H}\mathbf{d}+\mathbf{n})\left(\mathbf{d}^{\mathrm{H}}\mathbf{H}^{\mathrm{H}}+\mathbf{n}^{\mathrm{H}}\right)\right]\\ &= \mathrm{E}\left[-2\mathbf{H}\mathbf{d}\mathbf{d}^{\mathrm{H}}-2\mathbf{n}\mathbf{d}^{\mathrm{H}}+2\mathbf{W}\mathbf{H}\mathbf{d}\mathbf{d}^{\mathrm{H}}\mathbf{H}^{\mathrm{H}}\right.\\ &\qquad \left.+2\mathbf{W}\mathbf{n}\mathbf{d}^{\mathrm{H}}\mathbf{H}^{\mathrm{H}}+2\mathbf{W}\mathbf{H}\mathbf{d}\mathbf{n}^{\mathrm{H}}+2\mathbf{W}\mathbf{n}\mathbf{n}^{\mathrm{H}}\right].\end{aligned} \tag{3.53}$$

Since the signal and noise are uncorrelated, the expression can be reduced to

$$\frac{\mathrm{d}}{\mathrm{d}\mathbf{W}}\epsilon^2 = \mathrm{E}\left[-2\mathbf{H}\mathbf{d}\mathbf{d}^{\mathrm{H}}+2\mathbf{W}\mathbf{H}\mathbf{d}\mathbf{d}^{\mathrm{H}}\mathbf{H}^{\mathrm{H}}+2\mathbf{W}\mathbf{n}\mathbf{n}^{\mathrm{H}}\right]. \tag{3.54}$$

To find the minimum mean squared error ϵ^2, this function must equal zero, as

$$\mathrm{E}\left[-\mathbf{H}\mathbf{d}\mathbf{d}^{\mathrm{H}}+\mathbf{W}\mathbf{H}\mathbf{d}\mathbf{d}^{\mathrm{H}}\mathbf{H}^{\mathrm{H}}+\mathbf{W}\mathbf{n}\mathbf{n}^{\mathrm{H}}\right]=0. \tag{3.55}$$

Since both the transmitted symbols and the noise can each be considered uncorrelated in space, $\mathrm{E}\left[\mathbf{d}\mathbf{d}^{\mathrm{H}}\right]=\sigma_d^2\mathbf{I}$ and $\mathrm{E}\left[\mathbf{n}\mathbf{n}^{\mathrm{H}}\right]=\sigma_n^2\mathbf{I}$, with $\mathbf{I}$ being the identity matrix. The equation can then be presented as

$$\begin{aligned}0 &= -\sigma_d^2\mathbf{H}+\sigma_d^2\mathbf{W}\mathbf{H}\mathbf{H}^{\mathrm{H}}+\sigma_n^2\mathbf{W}\\ &\downarrow\\ \sigma_d^2\mathbf{H} &= \sigma_d^2\mathbf{W}\mathbf{H}\mathbf{H}^{\mathrm{H}}+\sigma_n^2\mathbf{W}\\ &\downarrow\\ \mathbf{W} &= \sigma_d^2\mathbf{H}\left(\sigma_d^2\mathbf{H}\mathbf{H}^{\mathrm{H}}+\sigma_n^2\mathbf{I}\right)^{-1}\end{aligned} \tag{3.56}$$

[11] Mean Square Error

Since $N_{\mathrm{Rx}} \leq N_{\mathrm{Tx}}$ the Matrix Inversion Lemma must be applied to permit the matrix operation $\mathbf{y} = \mathbf{W}\mathbf{z}$[10, p. 88]. Furthermore, since the average energy of the signal σ_d^2 can be normalized to one and $\sigma_n^2 = N_0$, the MMSE[12] expression thus becomes

$$\mathbf{W} = \left(\mathbf{H}^{\mathrm{H}}\mathbf{H} + N_0\mathbf{I}\right)^{-1}\mathbf{H}^{\mathrm{H}} \tag{3.57}$$

3.6.3 Successive interference cancellation

A method to improve performance of ZF and MMSE is to decode one symbol at a time and use the information from the detected symbols to reduce the interference on the remaining ones. The procedure used in this project is as follows:

1. Equalize symbol # by using ZF/MMSE and do hard detection.
2. Re-encode the symbol.
3. Subtract the re-encoded symbol from the received symbol vector z.
4. Remove the channel coefficients belonging to symbol #.

The procedure must be iterated through all symbols, and relies on a correct detection of the already decoded symbols.

In the following, ZF in a 2×2 system is extended to ZF-SIC[13], using the above procedure. First the channel estimation matrix is modified by removing the channel coefficients belonging to the correctly decoded symbol ($\mathrm{desc}\langle y_1 \rangle$) as

$$\mathbf{H} = \begin{bmatrix} h_{11} & h_{12} \\ h_{21} & h_{22} \end{bmatrix} \rightarrow \mathbf{H} = \begin{bmatrix} h_{12} \\ h_{22} \end{bmatrix} \tag{3.58}$$

so that the channel inverse is

$$\begin{aligned} \mathbf{W} &= \left(\begin{bmatrix} \overline{h_{12}} & \overline{h_{22}} \end{bmatrix} \cdot \begin{bmatrix} h_{12} \\ h_{22} \end{bmatrix} \right)^{-1} \cdot \begin{bmatrix} \overline{h_{12}} & \overline{h_{22}} \end{bmatrix} \\ &= \frac{1}{\overline{h_{12}} \cdot h_{12} + \overline{h_{22}} \cdot h_{22}} \cdot \begin{bmatrix} \overline{h_{12}} & \overline{h_{22}} \end{bmatrix}. \end{aligned} \tag{3.59}$$

Next, the received symbol vector is modified:

$$\mathbf{z} = \begin{bmatrix} h_{11} \cdot d_1 + h_{12}d_2 - h_{11} \cdot \mathrm{desc}\langle y_1 \rangle + n_1 \\ h_{21} \cdot d_1 + h_{22}d_2 - h_{21} \cdot \mathrm{desc}\langle y_1 \rangle + n_2 \end{bmatrix} \tag{3.60}$$

[12]Minimum Mean Square Estimater
[13]Successive Interference Cancellation

with desc $\langle\cdot\rangle$ being the hard decision of the given received symbol. Finally, y_2 is equalized as

$$\begin{aligned}
y_2 &= \frac{1}{\overline{h_{12}} \cdot h_{12} + \overline{h_{22}} \cdot h_{22}} \cdot \begin{bmatrix} \overline{h_{12}} & \overline{h_{22}} \end{bmatrix} \cdot \begin{bmatrix} h_{12} \cdot d_2 + n_1 \\ h_{22} \cdot d_2 + n_2 \end{bmatrix} \\
&= \frac{\overline{h_{12}} \cdot (h_{12} \cdot d_2 + n_1) + \overline{h_{22}} \cdot (h_{22} \cdot d_2 + n_2)}{\overline{h_{12}} \cdot h_{12} + \overline{h_{22}} \cdot h_{22}} \\
&= d_2 + \frac{\overline{h_{12}} \cdot n_1 + \overline{h_{22}} \cdot n_2}{\overline{h_{12}} \cdot h_{12} + \overline{h_{22}} \cdot h_{22}}
\end{aligned} \tag{3.61}$$

which is recognized as the MRC decoder for d_2, described in section 3.4, which is known to be the optimal decoder for a SIMO system.

A further extension to SIC is OSIC[14], in which the channel estimate is used to find the optimal order of symbol equalization. Defining $\mathbf{P} = \mathbf{W}\mathbf{W}^{\mathrm{H}}$ as the covariance matrix of the channel equalizer, the equalization order is then defined by starting with the symbols having the least error variance, i.e. the lowest value on the diagonal entry of $\mathbf{P}$.

3.6.4 Maximum likelihood

The optimal method to decode spatially multiplexed symbols is to perform an exhaustive search for the minimum error

$$\mathbf{y} = \min_{\mathbf{d} \in \mathrm{O}_{\mathbf{d}}} |\mathbf{z} - \mathbf{H}\mathbf{d}|^2 \tag{3.62}$$

with $\mathrm{O}_{\mathbf{d}}$ containing the $M^{N_{\mathrm{Tx}}}$ possible symbol combinations in the spatial domain. This method, however, becomes very heavy from a computational perspective, as the complexity rises exponentially with the number of symbols in the symbol constellation and the number of spatial streams in the transmission[11].

3.6.5 Performance of SMUX receiver algorithms

The following figures illustrate the performance of the MIMO receiver algorithms. The simulations are done using OFDM modulated symbols transmitted through a narrowband i.i.d. Rayleigh fading channel with an accurate channel estimation at the receiver. The plots are equal to plots in [10, p. 99-101] and [12], although these references use SNR per receive antenna on the x-axis, while the simulations in this section use $\mathcal{E}_b/N_0$.

In figure 3.11, the BER of a 2×2 system with QPSK modulated symbols is shown. Because SMUX[15] is utilized, two symbols are transmitted at each symbol time. As stated in [10, p. 81], the diversity order of ZF and MMSE is $N_{\mathrm{Rx}} - N_{\mathrm{Tx}} + 1 = 1$, whereas the ZF-OSIC and especially MMSE-OSIC gain some diversity in the low SNR regime[11, fig. 8.7]. The diversity order of ML is stable at $N_{\mathrm{Rx}} = 2$[11, p. 95] and slightly better than MMSE-OSIC, even at low SNR.

[14] Ordered Successive Interference Cancellation

[15] Spatial Multiplexing

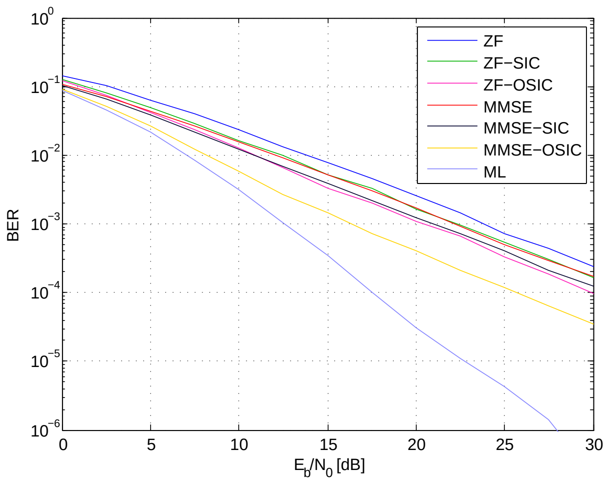

Figure 3.11: BER of QPSK signal in a 2×2 antenna system with different SMUX equalizers.

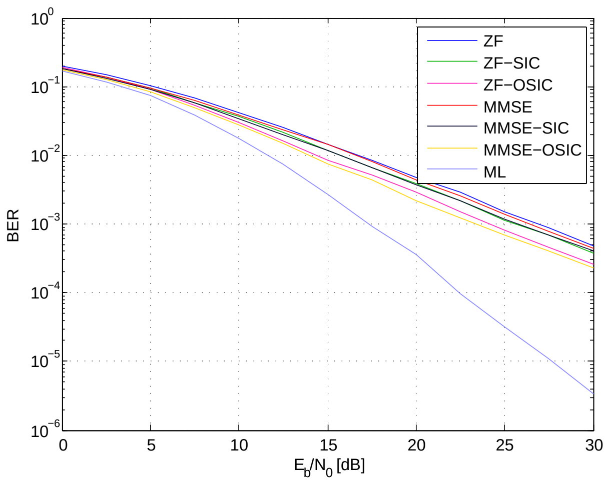

Figure 3.12: BER of 16-QAM signal in a 2×2 antenna system with different SMUX equalizers.

In figure 3.12, the simulation is run with same conditions as in figure 3.11, but with a modulation order of 16-QAM. Most significant is the change in diversity gain of the MMSE-OSIC, which is lost due to the greater possibility of wrong decoding of the first symbol in the sequence. This seriously diminishes the possibility of decoding the rest of the symbols correctly[10, p. 100]. MMSE-OSIC has almost no advantage compared to ZF-OSIC, whereas ML still sustains the theoretical diversity gain of $N_{\mathrm{Rx}} = 2$.

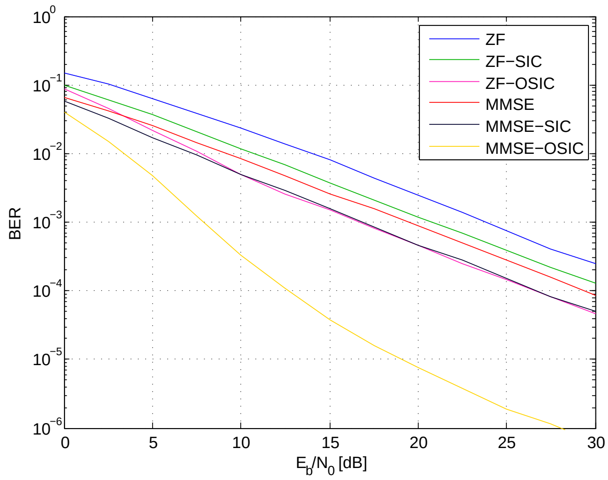

Figure 3.13: BER of QPSK signal in a 4×4 antenna system with different SMUX equalizers.

Figure 3.13 and 3.14 show simulations of BER in a 4×4 i.i.d. Rayleigh fading channel with modulation orders QPSK and 16-QAM. Again, the diversity gain of the ZF and MMSE receiver algorithm in all simulations is 1. For the QPSK simulation, the MMSE-OSIC has a significantly better performance than all other equalizers, whereas ZF-OSIC in the 16-QAM case slightly outperforms every receiver algorithm except from the MMSE-OSIC in the high SNR regime.

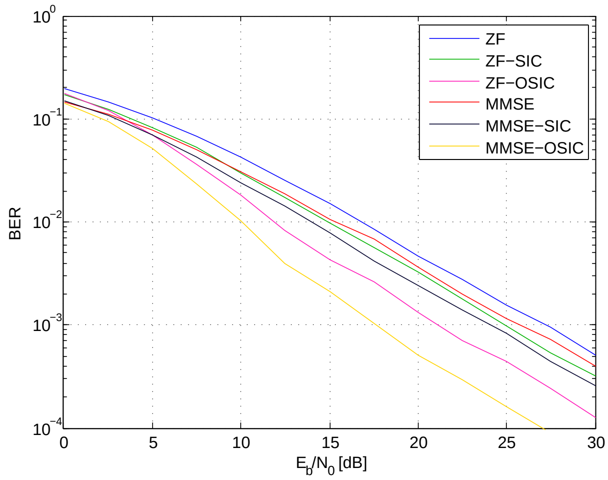

Figure 3.14: BER of 16-QAM signal in a 4×4 antenna system with different SMUX equalizers.

In 3.15 a simulation in a 4×2 i.i.d Rayleigh channel is shown. In this simulation, all equalizers obtain additional diversity gain compared to the simulations in 2×2 and 4×4 case, because 4 antennas are used to collect 2 spatial streams. As expected, the diversity gain of ZF is around $N_{\mathrm{Rx}} - N_{\mathrm{Tx}} + 1 = 3$, giving a significantly better performance compared to having only 2 receive antennas.

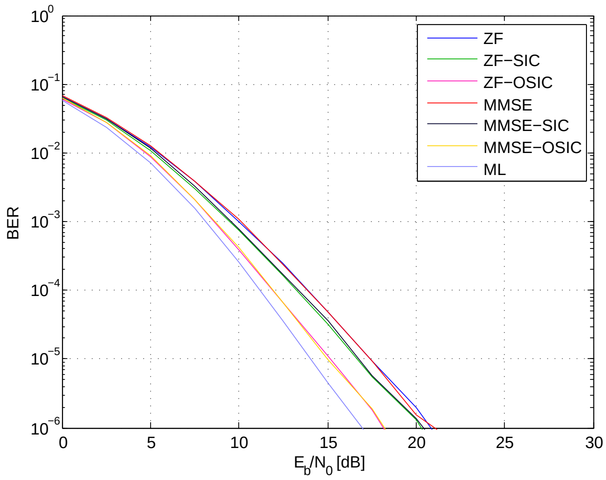

Figure 3.15: BER of 16-QAM signal in a 4 × 2 antenna system with different SMUX equalizers.

3.7 Summary

In this chapter, the structure of the MIMO channel and receiver algorithms have been described thoroughly. It has been shown how the receiver can gain performance by adding multiple antennas, and how a system can increase the throughput by utilizing the extra degrees of freedom gained by adding multiple antennas at both the transmitter and at the receiver. To comply with the latest mobile communication standards, the study focused on OFDM modulated systems. Lastly, it is seen by evaluation of the described receivers, that MMSE-OSIC and ML achieve the highest performance when utilizing spatial multiplexing. Since ML is very heavy from at computational perspective and thereby not feasible to implement in a physical receiver, MMSE-OSIC is chosen as reference receiver in the following chapters. However, when performance comparison is needed, MMSE will also be used.

Chapter 4

Turbo coding and rate matching

To maximize the throughput of a modern transmission system, redundant data is added to the information. Current communication systems implement Turbo codes, which will be described in this chapter. Furthermore, simulations with coding will be run to show throughput when utilizing the channel coding techniques for LTE.

A Turbo code is created by feeding two parallel concatenated convolutional encoders with respectively the information stream and an interleaved version of the same. The output of a Turbo encoder is the information stream itself, together with the two outputs from the convolutional encoders. The outputs are combined to a single bit stream before modulation. To comply with the current channel properties, the output punctured to change the code rate and thereby the maximum throughput. The structure of a Turbo encoder is shown in figure 4.1, which also includes the sub block interleavers and a multiplexing block which combines the streams from the encoders and possibly changes the code rate.

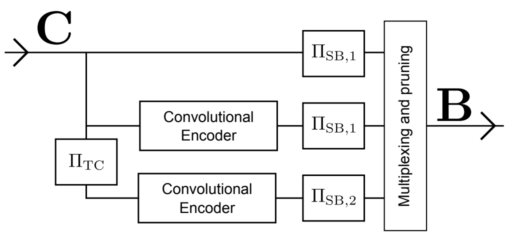

Figure 4.1: Turbo encoder block diagram. For simplicity, the systematic output of the convolutional encoders are not shown.

4.1 Convolutional codes

Convolutional coding is a FEC[1] technique which encapsulates m bits of information into n bits by adding redundancy[13]. The encoded bit stream thereby

[1]Forward Error Correcting

has a code rate m/n. The type of convolutional encoder used for Turbo codes is a recursive systematic encoder, with the keyword *recursive* indicating that one of the convolutions in the encoder are fed back to the input of the encoder, while the *systematic* keyword defines that the input is used directly as an output of the encoder.

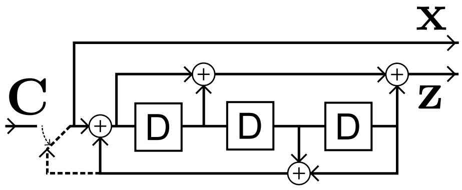

Figure 4.2: Recursive systematic encoder used in LTE. The arrow and the dotted lines show the configuration when creating terminating bits

The encoder used in LTE, is an encoder based on the polynomials $\mathbf{g}_1 = [1\ 0\ 1\ 1]$ and $\mathbf{g}_r = [1\ 1\ 0\ 1]$, which defines the additions in the implementation of the encoder, shown in figure 4.2. The blocks in the encoder are buffer elements, and the addition elements correspond to modulo-2 additions (X-OR operations). The switch in the left side of the figure illustrates the change which happens to the encoder when the all information bits $x_0, x_1, .., x_K$ are encoded, and termination of the transmission stream starts.

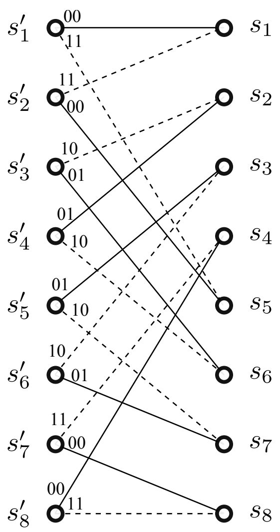

Figure 4.3: Trellis diagram for LTE Turbo codes

In figure 4.3, the trellis diagram corresponding to the LTE Turbo code convolutional encoders are shown. The left-side dots represent the states (content of buffer elements in the encoder) s'_j in which the convolutional encoder is before the current transition. The solid lines represent that a message bit 0 is transmitted, while the dotted lines represent a 1. The numbers attached to each line represent the transmitted bits for each transition. The state s_k represent the state in which the encoder will be after encoding the current message bit.

As an example, if the encoder is in state s'_2, and a message bit 0 is to be encoded, the encoder will output 00 for transmission and go to the state s_5, after which the process will start all over again. The encoder always starts encoding of a new frame from the state s'_1. Not all states will thus be accessible until the fourth transition. The termination of the frame, on the other hand, ensures that the encoder will always return to the state s_1.

4.2 Encoding of Turbo codes

As illustrated in figure 4.1, two convolutional encoders of the type described in the previous section, are combined by the use of an interleaver to create an output with code rate 1/3. Beside the parity outputs, the systematic termination outputs from the encoders are supplied to the multiplexer.

The Turbo code interleaver used in LTE is a QPP[2] interleaver, which uses the second order polynomial

$$\Pi_{\mathrm{TC}}[i] = (f_1 i + f_2 i^2) \bmod K \tag{4.1}$$

with K being the frame length, and f_1, f_2 being integer numbers defined for each LTE frame length[14, sec. 5.1.3]. The interleaver enables a multi thread decoder to utilize dual access RAM for decreasing the decoding delay in the receiver. The outputs from the Turbo encoder is denoted $\mathbf{x}'$ as the interleaved systematic output and $\mathbf{z}'$ as the interleaved parity output.

4.3 Multiplexing and rate matching

Turbo codes ensure that the information can be decoded to a BER below 10^{-5} even with an uncoded BER above 10^{-1}[13, fig. 6.3]. On the downside, Turbo coding raises the bandwidth requirements to 3 times the uncoded case, which is inconvenient if the uncoded BER is low. Therefore, techniques have been developed, so that the encoded stream can be punctured to change the code rate. This, along with a change in modulation order on behalf of the present channel quality, is known as rate matching. For LTE, this technique makes it able to vary the maximal physical layer throughput from 0.15 to 5.6 bits/Hz/sec[15, tab. 10.1] without utilizing SMUX.

In LTE, the output from the Turbo encoder is packed into three streams, $\mathbf{b}^{(0)}$, $\mathbf{b}^{(1)}$ and $\mathbf{b}^{(2)}$ as

$$\mathbf{b}^{(0)}_{0:K-1} = \mathbf{x}_{0:K-1} \tag{4.2}$$

$$\mathbf{b}^{(1)}_{0:K-1} = \mathbf{z}_{0:K-1} \tag{4.3}$$

$$\mathbf{b}^{(2)}_{0:K-1} = \mathbf{z'}_{0:K-1} \tag{4.4}$$

$$\begin{array}{llll}
b^{(0)}_{K} = x_K & b^{(0)}_{K+1} = z_{K+1} & b^{(0)}_{K+2} = x'_K & b^{(0)}_{K+3} = z'_{K+1} \\
b^{(1)}_{K} = z_K & b^{(1)}_{K+1} = x_{K+2} & b^{(1)}_{K+2} = z'_K & b^{(1)}_{K+3} = x'_{K+2} \\
b^{(2)}_{K} = x_{K+1} & b^{(2)}_{K+1} = z_{K+2} & b^{(2)}_{K+2} = x'_{K+1} & b^{(2)}_{K+3} = z'_{K+2}
\end{array}$$

Before the interleaveing process, preceding dummy bits are padded until the length D of the arrays modulus 32 equals 0. $\mathbf{b}^{(0)}$ and $\mathbf{b}^{(1)}$ are then interleaved by a block interleaver with 32 columns[14, sec. 5.1.4]. The padded arrays are written row-wise into a $({}^{D}\!/_{32} \times 32)$ matrix, which undergoes column permutation, after which the data is read out column by column. This defines the interleaver as

$$\Pi_{\mathrm{SB},1}[i] = P_{\lfloor i/R \rfloor} + 32 \cdot (i \bmod R) \tag{4.5}$$

[2]Quadratic Permutation Polynomial

with P being the column permutation order, and R being the number of rows in the matrix defined as

$$\begin{aligned} P = (&0,\ 16,\ 8,\ 24,\ 4,\ 20,\ 12,\ 28,\ 2,\ 18,\ 10,\ 26,\ 6,\ 22,\ 14,\ 30,\\ &1,\ 17,\ 9,\ 25,\ 5,\ 21,\ 13,\ 29,\ 3,\ 19,\ 11,\ 27,\ 7,\ 23,\ 15,\ 31)\\ R = &D/32. \end{aligned} \tag{4.6}$$

The interleaver for $\mathbf{b}^{(2)}$ is chosen differently, and is defined by

$$\Pi_{\mathrm{SB},2}[i] = \left(P_{\lfloor i/R \rfloor} + 32 \cdot (i \bmod R) + 1\right) \mod D \tag{4.7}$$

Finally, the interleaved bit streams are multiplexed into a single array $\mathbf{b}'$ as

$$\mathbf{b}'_{0:D-1} = \mathbf{b}^{(0)}_{\Pi_{\mathrm{SB},1}[0:D-1]} \tag{4.8}$$

$$\mathbf{b}'_{D,D+2:3D-2} = \mathbf{b}^{(1)}_{\Pi_{\mathrm{SB},1}[0:D-1]} \tag{4.9}$$

$$\mathbf{b}'_{D+1,D+3:3D-1} = \mathbf{b}^{(2)}_{\Pi_{\mathrm{SB},2}[0:D-1]} \tag{4.10}$$

where it is seen that the array $\mathbf{b}'$ is created by writing the interleaved version of $\mathbf{b}^{(0)}$ into the first part of the array, while interleaved versions of $\mathbf{b}^{(1)}$ and $\mathbf{b}^{(2)}$ are written alternately into the last part of the array. $\mathbf{b}'$ is then ready to be punctured and modulated. The puncturing is performed by choosing the starting point of the stream to be index $i_0 = 2R$ and then modulate the part of the bit stream defined by the code rate. The bits are read out forward in the array $\mathbf{b}'$. The dummy bits inserted during the sub block interleaving is not to be transmitted and must be skipped. Code rates lower than 1/3 can be reached by transmitting the same bits more than once, by continue reading from the beginning of the array when reaching the end.

4.4 Decoding of Turbo codes

The algorithm needed to decode a Turbo encoded sequence is significantly more complicated compared to the one used for the encoding it. The commonly used decoder consists of two parallel BCJR[3] convolutional decoders. These operate iteratively by exchanging extrisic information, to estimate the transmitted information.

To gain maximum performance from the iterative decoder, a soft decision bit stream is needed as input. The sign of a soft bit indicates whether a received bit is estimated as a 1 or a 0, while the amplitude of the value indicates the reliability of the estimation. A common method is to calculate the LLR[4], $\hat{b}_k$, of the transmitted symbols by[16, 17]:

$$\hat{b}_k = \ln \frac{\sum P\left[b_k = 1|d\right]}{\sum P\left[b_k = 0|d\right]} \tag{4.11}$$

$$= \ln \frac{\sum_{s\in S_1} \exp\left(SNR\left((d_I - s_I)^2 + (d_Q - s_Q)^2\right)\right)}{\sum_{s\in S_0} \exp\left(SNR\left((d_I - s_I)^2 + (d_Q - s_Q)^2\right)\right)} \tag{4.12}$$

[3]Bahl-Cocke-Jelinek-Raviv

[4]Log-likelihood Ratio

with $SNR = |h|^2 \frac{\mathcal{E}_b}{N_0}$. Equation (4.11) defines the total probability of having received respectively 1 and 0 from the received symbol. Equation (4.12) calculates the probablilities as the squared euclidian distance from the received symbol to each possible symbols indicating respectively 1 and 0, with the SNR taken into account.

In figure 4.4, the 16-QAM constellation diagram is shown. It can be observed that a particular bit depends only on the real or the imaginary value of the symbol, meaning that the two parts of a received symbol can be used independently when deriving the soft bits. In [16], a simple soft decision demodulator for QAM modulation schemes is suggested. The demodulator calculates the euclidian distance from the equalized symbol to the hard decision lines in the constellation on a per bit basis. The method is proven to have very little performance degradation when compared to LLR.

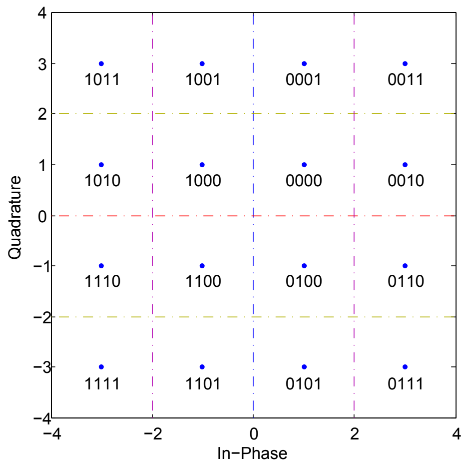

Figure 4.4: The constellation diagram for 16-QAM used in LTE. The dashed lines show the hard decision rules for the demodulator. The blue line represents the first bit, the red line represents the second bit, the purple lines prepresent the third bit and the yellow lines represent the fourth bit.

For the case of 16-QAM, the four bits are calculated as

$$\hat{b}_{4i} = -\left|\mathrm{Re}\left(y_i\right)\right| |h|^2 \tag{4.13}$$
$$\hat{b}_{4i+1} = -\left|\mathrm{Im}\left(y_i\right)\right| |h|^2 \tag{4.14}$$
$$\hat{b}_{4i+2} = \left(\left|\mathrm{Re}\left(y_i\right)\right| - 2\right) |h|^2 \tag{4.15}$$
$$\hat{b}_{4i+3} = \left(\left|\mathrm{Im}\left(y_i\right)\right| - 2\right) |h|^2 \tag{4.16}$$

A similar procedure is used for calculating soft decision outputs for BPSK, QPSK and 64-QAM.

When the received symbols have been demodulated, these must be demultiplexed and deinterleaved according to section 4.3. The output from the demultiplexers, with additional zeros to represent bits which have not been transmitted, is then fed to the Turbo decoder. The Turbo decoder consists of two

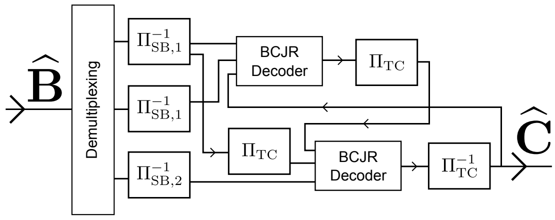

Figure 4.5: Turbo decoder block diagram.

parallel BCJR decoders which handle the non-interleaved and the interleaved bitstream separately. This structure is shown in figure 4.5. An interleaver is introduced between the systematic stream and the interleaved decoder, since an interleaved version of the systematic stream is included in the transmitted bit stream. Finally, the extrinsic output from the decoders, which is zero at the first iteration, is fed through a (de)interleaver to produce the input for the following decoder in the iteration.

The BCJR decoder calculates the soft output based on the systematic and the parity inputs. Combined with intrinsic information from the iterative process the LLR of the of transmitted symbols as

$$L(\hat{c}_i|\mathbf{y}) = \ln \frac{P(c_i = +1|\mathbf{y})}{P(c_i = -1|\mathbf{y})} \tag{4.17}$$

where $P(\cdot)$ represents an a priori probability that the given bit have been transmitted. The probabilities are defined as

$$L(\hat{c}_i|\mathbf{y}) = \ln \frac{\sum_{R_1} \alpha_{i-1}(s'_j)\gamma_i(s'_j, s_k)\beta_i(s)}{\sum_{R_0} \alpha_{i-1}(s'_j)\gamma_i(s'_j, s_k)\beta_i(s_k)} \tag{4.18}$$

with $\alpha_{i-1}(s'_j)$ being the forward recursive probability to be in state s'_j before the ongoing transition, $\beta_i(s_k)$ is the backward recursive probability to be in state s_k after the current transition, while $\gamma_i(s'_j, s_k)$ is the probability that the given transition is taking place. R_1 includes all state transitions that indicates a message bit 1, while R_0 includes all transitions that indicates that a 0 has been transmitted. A thorough description of the BCJR decoder can be found in [13].

4.5 Evaluation of channel coding

This section presents simulations of throughput for systems with Turbo coding and rate matching as defined in this chapter. For SMUX, the MMSE-OSIC equalizer is used. HARQ is not utilized. All simulations in this section are done with OFDM over 8 subcarriers and a total of 1024 modulated symbols per frame.

In figure 4.6 the throughput for a SISO system without fading is seen. The simulation matches results in [18]. The simulation shows the advantage of adaptive coding, as the throughput can be maximized for any SNR by choosing the optimal code rate.

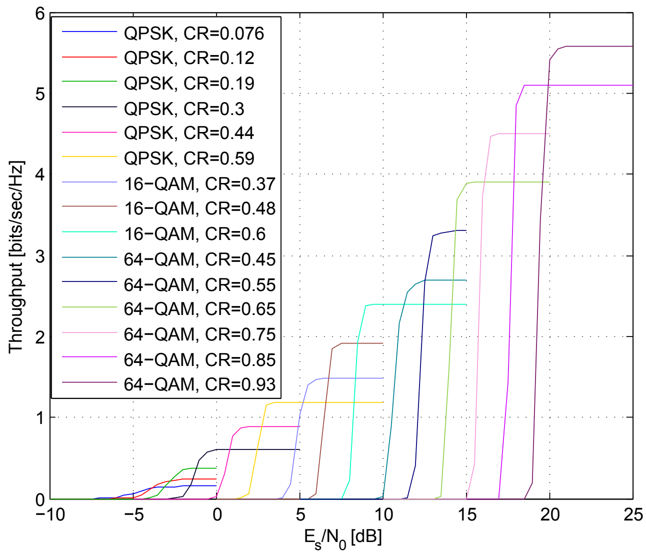

Figure 4.6: Performance in a SISO system in an uncorrelated Rayleigh fading channel.

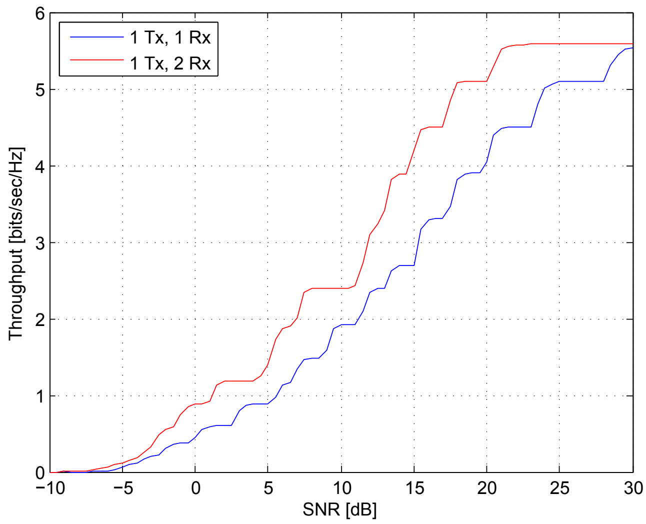

Figure 4.7: Performance in a SISO system in an uncorrelated Rayleigh fading channel.

In figure 4.7, a maximum throughput simulation in a Rayleigh channel using respectively 1 and 2 receive antenna elements is shown. It is clear that the line utilizing diversity has a steeper ascent, matching the effect seen in the BER simulations in figure 3.4.

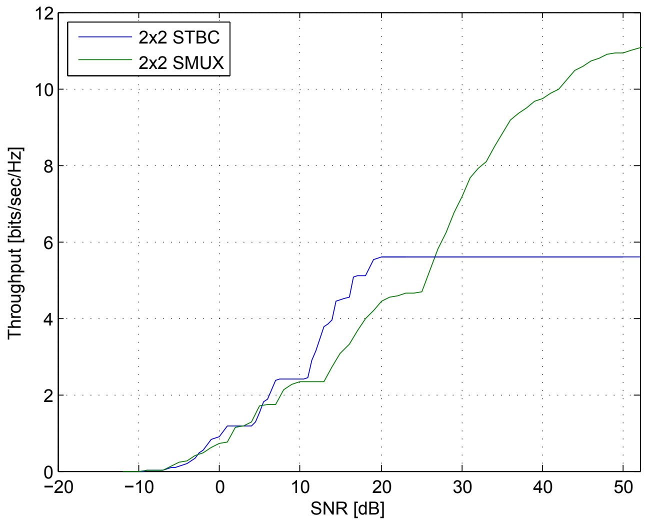

Figure 4.8: SMUX and STBC maximum performance in a 2×2 system in an uncorrelated Rayleigh fading channel.

In figure 4.8, a maximum throughput simulation for a 2×2 Rayleigh channel using respectively STBC and SMUX is shown. It is seen that for the low SNR regime, STBC outperforms SMUX because of a higher diversity gain. SMUX in return is able to give a higher throughput for high SNRs, as STBC has a theoretical maximum of approximately 5.8 bit/sec/Hz. The lines in figure 4.8 are directly comparable, as the transmitter is able to choose transmission mode from the channel quality to gain maximal throughput. The simulations are shown such that the same energy is in both cases. This makes the SNR of STBC being ${}^{\mathcal{E}_s}/_{N_0}$, and the SNR of SMUX being $\frac{\mathcal{E}_s/2}{N_0}$.

4.6 Summary

In this chapter, channel coding in form of Turbo codes with rate matching complying to LTE, has been analyzed. Simulations of throughput showed how SMUX is able to raise the limit of total throughput, while STBC has a better performance in low SNR regime, as it is able to utilize a higher diversity gain of the channel.

Chapter 5

Spatially correlated channel models

In real world communications, a form of correlation between MIMO subchannels is expected. This correlation degrades channel quality and thereby the BER at the receiver end. For diversity transmissions, correlation reduces the advantages of having multiple receive antennas; the diversity gain goes towards zero as the correlation rises. When considering MIMO and SMUX with CSI[1] only at the receiver, the effects are even more remarkable. In this case, correlation can completely hinder the possibility of recreating any of the transmitted symbols. To simulate MIMO correlation, several models have been defined. Some of these models will be presented in the following, and a simple spatial channel model then will be developed.

5.1 Full-correlation model

The correlation of any channel can be described by using the matrix[1]

$$\mathbf{R}_{\mathbf{H_c}} = \mathrm{E}\left[\mathrm{vec}\left(\mathbf{H_c}\right)\mathrm{vec}\left({\mathbf{H_c}}^{\mathrm{H}}\right)\right] \tag{5.1}$$

where $\mathbf{H_c}$ is the correlated channel matrix and with $\mathrm{vec}(\cdot)$ being the operator that stacks the columns in the matrix. The model contains values to describe the correlation between every channel coefficient and every other channel coefficient in the channel matrix. $\mathbf{R}_{\mathbf{H_c}}$ is obviously hermitian by nature.

The model can be used in simulations by imposing that

$$\mathbf{H}_c = \mathrm{unvec}\left(\mathbf{R}_{\mathbf{H_c}}^{1/2}\mathrm{vec}(\mathbf{H})\right) \tag{5.2}$$

with $\mathbf{H}$ being an i.i.d. Rayleigh channel matrix. Its employment requires $(1 + N_{\mathrm{Rx}}N_{\mathrm{Tx}})\frac{N_{\mathrm{Rx}}N_{\mathrm{Tx}}}{2}$ values.

5.2 Kronecker model

The Kronecker model[1] simplifies the Full-correlation model by the assumption that the scatters around the transmitter are uncorrelated with respect to these

[1] Channel State Information

around the receiver. A channel based on the Kronecker model is realized as

$$\mathbf{H}_c = \mathbf{R}_{\mathrm{Rx}}^{1/2}\mathbf{H}\mathbf{R}_{\mathrm{Tx}}^{1/2^{\mathrm{H}}}. \tag{5.3}$$

with $\mathbf{R}_{\mathrm{Rx}}$ and $\mathbf{R}_{\mathrm{Tx}}$ being matrices of size $N_{\mathrm{Rx}} \times N_{\mathrm{Rx}}$ and $N_{\mathrm{Tx}} \times N_{\mathrm{Tx}}$. The matrix $\mathbf{R}_{\mathbf{H}}$ can in turn be calculated from the Kronecker model as

$$\mathbf{R}_{\mathbf{H}} = \mathbf{R}_{\mathrm{Tx}}^{\mathrm{H}} \otimes \mathbf{R}_{\mathrm{Rx}} \tag{5.4}$$

The model needs $(1+N_{\mathrm{Rx}})\frac{N_{\mathrm{Rx}}}{2} + (1+N_{\mathrm{Tx}})\frac{N_{\mathrm{Tx}}}{2}$ coefficients to be implemented in a simulation. The model although have been criticized for being inadequate, particular when in MIMO systems larger than 2×2, as the scatters cannot be considered uncorrelated in a real communication system[19, 20].

5.2.1 Simplified Kronecker model

A simplification of the Kronecker model has been proposed in [10], by defining the correlation matrices as

$$\mathbf{R}_{\mathrm{Rx},ij} = X_{\mathrm{Rx}}^{|i-j|} \tag{5.5}$$

$$\mathbf{R}_{\mathrm{Tx},ij} = X_{\mathrm{Tx}}^{|i-j|} \tag{5.6}$$

with X_{Rx}, X_{Tx} being coefficients that can vary from 0 to 1 to create an uncorrelated and a completely correlated channel, respectively. For instance, a realization of the correlation matrices with $X_{\mathrm{Rx}} = 0.5$ is

$$\mathbf{R}_{\mathrm{Rx}} = \begin{bmatrix} 1.000 & 0.500 & 0.250 & 0.125 \\ 0.500 & 1.000 & 0.500 & 0.250 \\ 0.250 & 0.500 & 1.000 & 0.500 \\ 0.125 & 0.250 & 0.500 & 1.000 \end{bmatrix}. \tag{5.7}$$

5.2.2 Simulations with statistical fading

In figure 5.1, simulations with different coefficients of the simplified Kronecker correlation model are shown. For all simulations, it is seen that small coefficients have very little influence on the BER. Indeed when $X_{\mathrm{Rx}} = X_{\mathrm{Tx}} = 0.3$, the effect from correlation is nearly unnoticeable. Small changes in the correlation coefficients however have a large influence on the BER when the channel is highly correlated, seen from the difference between $X_{\mathrm{Rx}} = X_{\mathrm{Tx}} = 0.6$ and $X_{\mathrm{Rx}} = X_{\mathrm{Tx}} = 0.8$.

An aspect to notice is that the impact of correlation is equal for MMSE and MMSE-OSIC receivers. Furthermore, the degradation is independent of the modulation order. The loss in BER from correlation can be expressed as a negative power gain. As an example, the line in each plot representing $X_{\mathrm{Rx}} = X_{\mathrm{Tx}} = 0.6$ can be compared to the line with no correlation. Here it is seen that the correlation creates a constant offset of approximately 5 dB SNR, independent of modulation order and receiver algorithm.

Figure 5.1(d) shows a comparison of throughput between STBC and SMUX. It is clear that SMUX with spatial correlation has a decrease in throughput of approximately 5 dB as in the BER simulations, while STBC is able to sustain nearly the same performance with or without correlation, except from some loss in diversity gain at high SNR.

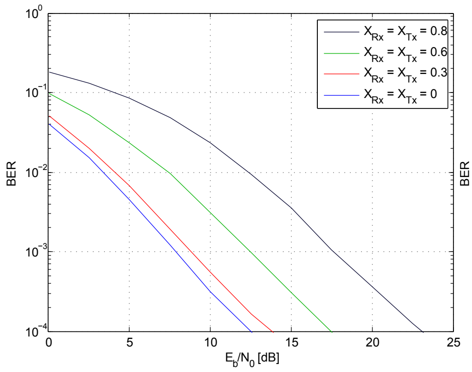

(a) QPSK, MMSE-OSIC

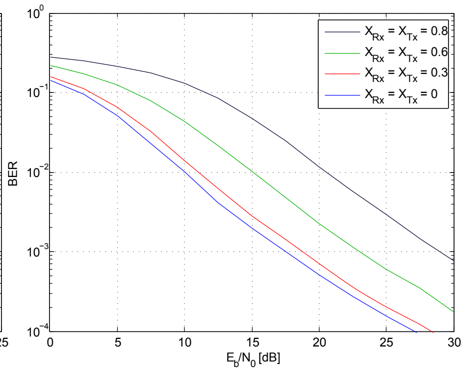

(b) 16-QAM, MMSE-OSIC

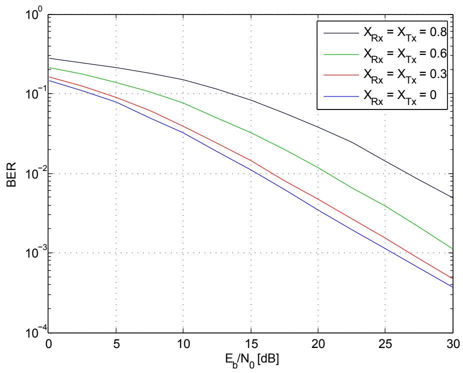

(c) 16-QAM, MMSE

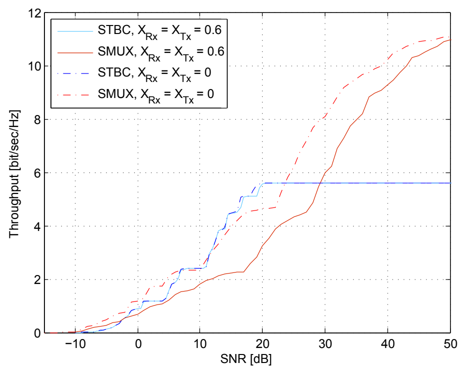

(d) MMSE-OSIC, 2×2

Figure 5.1: Impact on BER of channel correlation in a 4×4 channel.

5.3 IST WINNER II

From the previous sections, it can be concluded that methods to generate spatial correlation statistically are complicated to instantiate. The current channel models therefore generate channel coefficients based on geometrical constraints. The most sophisticated model available today is the WINNER[2] II channel model[21]. The model can be utilized in multicell environments, with links between several UE's, base stations, and relay stations[21, sec. 3.3]. The IST[3] network has created and published a MATLAB implementation of the model, [22].

The model can be utilized by defining a relatively small set of parameters. At a single link between a UE and a particular base station, the channel is created from reflections from clusters, as shown in figure 5.2, which each generates a sum of rays.

The equation for generating channel coefficients in WINNER II is given

[2] Wireless World Initiative New Radio
[3] Information Society Technologies

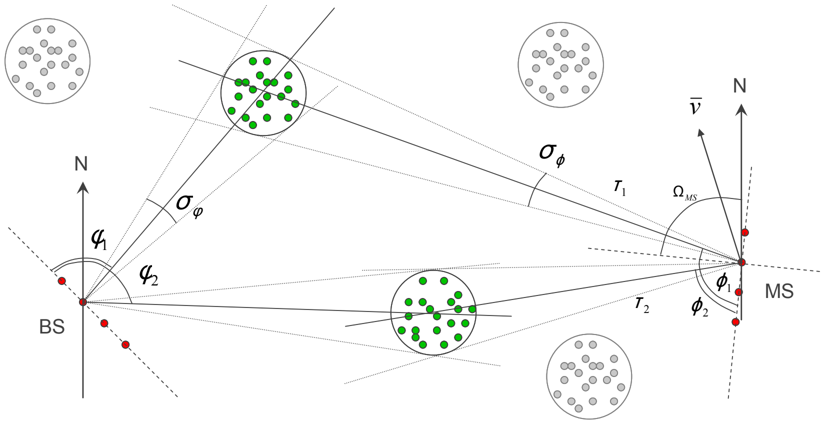

Figure 5.2: Single link in WINNER II channel specification, the figure illustrates the cluster-based approach. Figure is from [21].

by[21, eq. (4.14)]

$$
\begin{aligned}
\mathbf{H}_{u,s,n}(t) = {} & \sqrt{P_n} \sum_{m=1}^{M} \begin{bmatrix} F_{rx,u}^{V}(\varphi_{n,m}) \\ F_{rx,u}^{H}(\varphi_{n,m}) \end{bmatrix}^{\mathrm{T}} \\
& \cdot \begin{bmatrix} \exp\left(j\Phi_{n,m}^{vv}\right) & \sqrt{\kappa_{n,m}} \exp\left(j\Phi_{n,m}^{vh}\right) \\ \sqrt{\kappa_{n,m}} \exp\left(j\Phi_{n,m}^{hv}\right) & \exp\left(j\Phi_{n,m}^{hh}\right) \end{bmatrix} \begin{bmatrix} F_{tx,s}^{V}(\phi_{n,m}) \\ F_{tx,s}^{H}(\phi_{n,m}) \end{bmatrix} \\
& \cdot \exp\left(jd_s 2\pi\lambda_0^{-1} \sin\left(\phi_{n,m}\right)\right) \cdot \exp\left(jd_u 2\pi\lambda_0^{-1} \sin\left(\varphi_{n,m}\right)\right) \\
& \cdot \exp\left(j2\pi\lambda_0^{-1}\nu_{n,m} \cdot t\right)
\end{aligned} \tag{5.8}
$$

which is referred to the n^{th} ray. The first vector term in the summation is the receive antenna gain. The 2×2 matrix is the cross polarization matrix, while the second vector is the transmit antenna gain. The model suggests that if polarization is not considered, the cross polarization matrix can be replaced by a scalar phase contribution and scalar antenna gains, so that (5.8) is becomes

$$
\begin{aligned}
\mathbf{H}_{u,s,n}(t) = {} & \sum_{m=1}^{M} \sqrt{P_n} \exp\left(j\Phi_{n,m}\right) \\
& \cdot \exp\left(jd_s 2\pi\lambda_0^{-1} \sin\left(\phi_{n,m}\right)\right) \cdot \exp\left(jd_u 2\pi\lambda_0^{-1} \sin\left(\varphi_{n,m}\right)\right)
\end{aligned} \tag{5.9}
$$

which furthermore has the antenna patterns F_{rx} and F_{tx} removed, as the patterns is considered omnidirectional. Finally, the last term in eq. (5.8) is removed, as the antennas are assumed to be stationary.

Each ray consists of a sum of M sub-rays, defining the cluster-based approach. M is by definition equal to 20. Each sub-ray has a normal distributed transmit angle $\phi_{n,m}$ and receive angle $\varphi_{n,m}$ relative to the antenna array boresight, with a mean defined per cluster, and a standard deviation defined by the channel properties. The model adds a custom phase, uniformly distributed in range $[-\pi,\ \pi]$, per sub-ray by means of the parameter $\Phi_{n,m}$. The parameter d_s defines the distance from element 1 to element s and λ_0 defines the carrier wavelength.

The power per ray, with a exponential delay spread, is defined as[21, eq. (4.5)]

$$P'_n = \exp\left(-\tau_n \frac{r_\tau - 1}{r_\tau \sigma_\tau}\right) \cdot 10^{\frac{-Z_n}{10}} \tag{5.10}$$

with τ_n being the delay of the current ray, r_τ is the delay distribution proportionality factor and σ_τ is the delay spread. Z_n represents the shadow loss in dB, and is defined as $Z_n \sim \mathcal{N}(0, \zeta)$ with ζ defined per scenario to values from 3 to 8 dB.

5.4 Sandbox model

From previous section, it is seen that the AoD[4] and the AoA[5] are important parameters when defining the channel matrix. In this section, a deterministic, geometrically based channel model, usable for testing MIMO capabilities in a completely controlled environment, will be developed.

Antenna placements and angles of the rays are not limited by geometrical constraints. This implies that rays are plane waves at the receiver, as a consequence of the unknown distance between the transmitter and receiver. Only phases of the received rays vary due to different transmit and receive antennas in the arrays. An example of a given realization of the model is seen in figure 5.3.

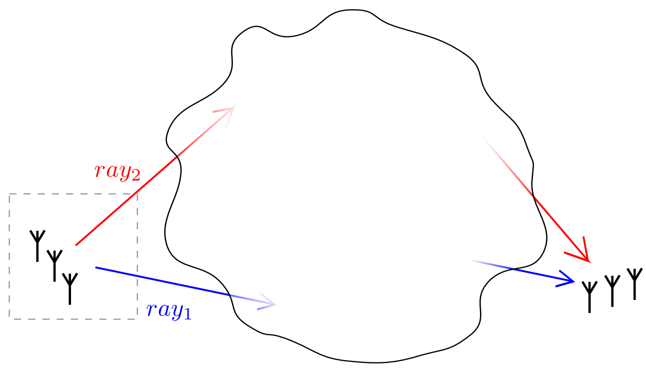

Figure 5.3: MIMO antenna system with two rays.

Figure 5.4 is a detailed version of the transmitter in figure 5.3. In the figure, some of the configurable options are shown. Φ_{Tx}, Δ_{Tx}, and N_{Tx} represent the angle, the distance between the antenna elements in wavelengths, and the number of antennas in each array. Each ray is represented by its transmit angle $\phi_{\text{Tx},n}$, its receive angle $\phi_{\text{Rx},n}$, its power a_n, and delay τ_n.

[4]Angle of Departure
[5]Angle of Arrival

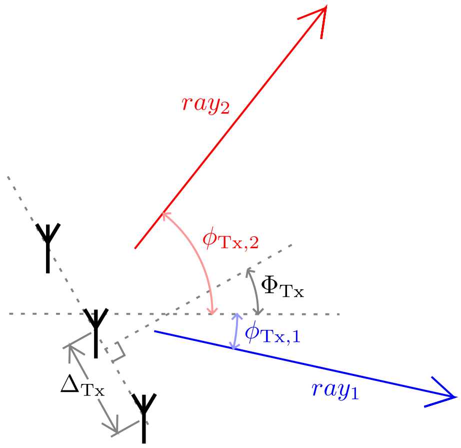

Figure 5.4: Detailed transmit part of figure 5.3.

The rays are defined on the basis of the afore mentioned properties as

$$\Omega_{\mathrm{Tx},n} = 2\pi \sin(\Phi_{\mathrm{Tx}} - \phi_{\mathrm{Tx},n}) \cdot \Delta_{\mathrm{Tx}} \tag{5.11}$$
$$\Omega_{\mathrm{Rx},n} = 2\pi \sin(\Phi_{\mathrm{Rx}} - \phi_{\mathrm{Rx},n}) \cdot \Delta_{\mathrm{Rx}} \tag{5.12}$$
$$\mathbf{G}_{u,s,n} = a_n \exp\left(j\Omega_{\mathrm{Tx},n}(s-1) + j\Omega_{\mathrm{Rx},n}(u-1)\right) \tag{5.13}$$

with $\Omega_{\mathrm{Tx},n}$ and $\Omega_{\mathrm{Rx},n}$ being the phase change between each antenna in the arrays, with the angle of the ray taken into consideration. $\mathbf{G}_{u,s,n}$ represents the coefficients developed from ray n. Finally, the rays are combined to a channel model as

$$\mathbf{G}_{u,s}(t) = \sum_n \mathbf{G}_{u,s,n} \delta(\tau_n - t) \tag{5.14}$$

5.4.1 Evaluation of Sandbox channel realizations

In this section, different scenarios configured in the Sandbox model will be evaluated with respect to the DCN[6], which is described in appendix C. The DCN expresses the invertibility of a matrix. In figure 5.5(b), the DCN for a 2×2 narrowband system is shown. One ray is fixed, and for the other, the AoD and the AoA are altered. Both rays have the same power. The distance between the elements is 1/2 of the wavelength and both arrays have their boresight at 0 degrees.

From figure 5.5(b) it is seen that the best invertibility is obtained when the rays are perpendicular to each other at transmitter and receiver. When the rays have the same or opposite AoD or AoA, the DCN instead tends to be large.

Figure 5.6(a) shows a DCN evaluation of the Sandbox model with Ray 2 having different power, i.e. $a_2 \in [-30,\ 30]$ dB. It is seen that large variations in the power can be accommodated as long as the angle between the rays is close to 90 degrees.

[6]Demmel Condition Number

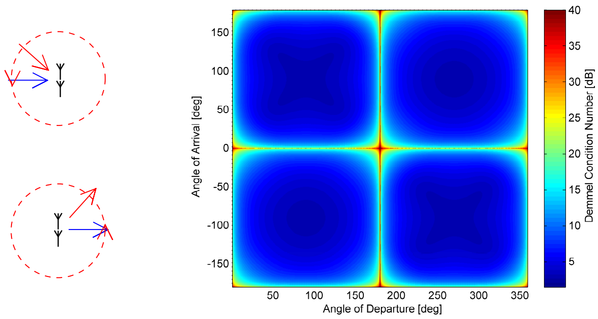

(a) **(b)** DCN

Figure 5.5: Sweep of AoD and AoD in Sandbox model. Ray 1 (blue) is kept constant, while Ray 2 (red) is sweeped from 0 – 360 deg (transmitter) and -180 – 180 deg (receiver).

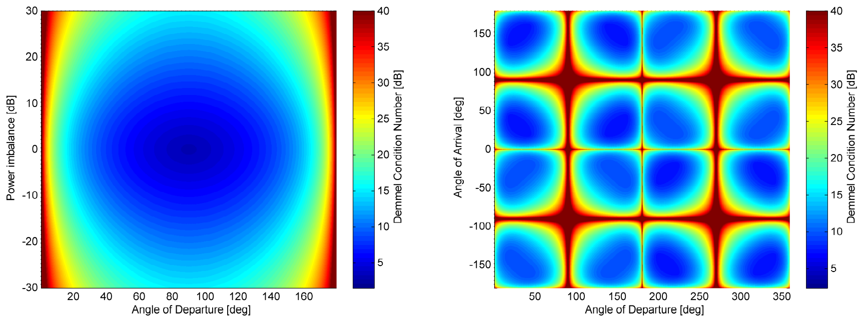

(a) 2 rays, one ray varying AoD and power

(b) 3 rays 1 ray varying AoD and AoA

Figure 5.6: DCN simulations with in a 2×2 channel (a) and a 3×3 channel (b).

In figure 5.6(b), a simulation with three elements per array is shown. Ray 1 and Ray 2 are fixed as two perpendicular rays, while Ray 3 is swept 360 deg at the transmitter and at the receiver. From this figure, it is clear that all angles have to be distinct to ensure the lowest DCN, and that having rays with near-equal angles are devastating, especially when ray angles is nearly perpendicular the angle of an antenna array.

5.4.2 Ring-model extension to Sandbox model

To ease simulations of geographically based scenarios, an interface which takes an additional set of parameters is developed for the Sandbox model. The extension is thus constrained to simulate only a subset of parameters possible in the Sandbox model. The LOS distance between the antennas must be configured, while the number of parameters per ray is reduced to include only the transmit angle and the ray traveling distance. The power per ray is calculated from the distance as

$$a_n = \frac{1}{d_n^2}. \tag{5.15}$$

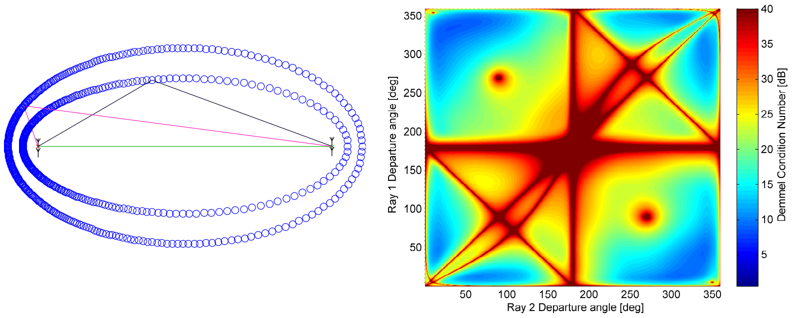

(a) Geometrical visualization

(b) DCN with rays like in (a)

Figure 5.7: DCN simulation with 1 LOS and 2 NLOS rays

Figure 5.7(a) shows the reflection points, which are calculated to keep the 2 NLOS[7] rays travel the constant defined distance. The distance traveled by Ray 1 and Ray 2 is 110 m and 120 m, respectively, while the LOS ray has a traveling distance of 100 m. 3 lines are added in figure 5.7(a) to illustrate a random realization of the channel with one ray representing the LOS ray and two other lines representing a ray with a reflecting point at a transmit angle of 30 deg and a traveling distance of 110 m and a ray with a reflecting point at 109 deg and a traveling distance of 120 m.

Figure 5.7(b) shows the DCN evaluation for a sweep as illustrated in figure 5.7(a). It is evident that the DCN typically is higher for the physically constrained sweep compared to the sweep in figure 5.6(b). The reason for this is that since the simulation sweep the transmit angles linearly, the receive angle closes the LOS receive angle for most transmit angles, as visualized in figure 5.7(a).

5.5 Adding stochastic properties to Sandbox model

In order to use the Sandbox model in BER simulations, some stochastic properties must be added to the channel. This is done by statistically vary the angles of the NLOS rays in a way similar to what has been proposed for the WINNER II model.

In figure 5.8, a simulation with the WINNER II model and the Extended Sandbox model is shown. The fading is configured such that the transmit angle of the NLOS rays have a standard deviation of 2 deg, while the receive angle

[7]Non-Line Of Sight

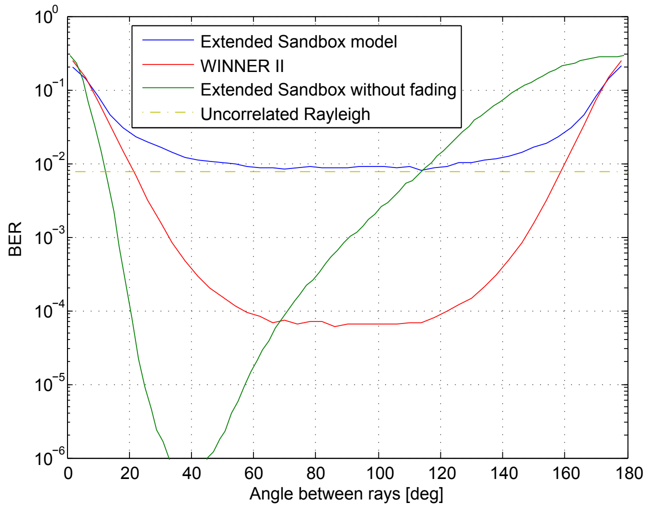

Figure 5.8: BER at $\mathcal{E}_b/N_0 = 15$ dB in a 2×2 16-QAM system using a MMSE-OSIC receiver with reflection point of second ray varying.

of the NLOS rays have a standard deviation of 10 deg. It is seen that the WINNER II channel model performs better, since the model uses the cluster based approach, which gives a higher spatial deviation and thereby a better conditioned channel. From figure 3.12, it is known that the BER in a Rayleigh channel with same parameters is $7 \cdot 10^{-3}$.

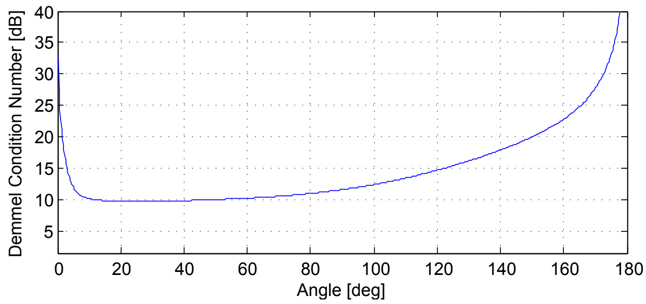

Figure 5.9: DCN of the extended Sandbox channel model with one NLOS ray varying its reflection point.

For comparison, a simulation with the Extended Sandbox model, without any fading added, is shown. From this, it is seen that the deterministic channel provides an excellent condition for an AoD between 20 degrees to 90 degrees. For lower AoDs, the spatial resolvability decreases because of a small deviation between the LOS and the NLOS AoD, while the AoA deviation shrinks for AoDs above 90 deg. Figure 5.9 shows the DCN for the Extended Sandbox model with same configuration.

The DCN in figure 5.9 does not completely relate to the BER simulation without fading, shown in figure 5.8. This is due to destructive interference between the rays from the affected transmit element, which lowers the SNR of the received signal from that element.

5.6 Summary

In this chapter, correlated channel models have been investigated. By adding statistical correlation to an i.i.d. Rayleigh channel model, it is concluded that STBC achieves further advantage in correlated channels, as SMUX is subjected to a significant negative power gain, while STBC is only vaguely affected.

From DCN evaluations in a deterministic channel model, it furthermore turns out that the AoDs and AoAs are of crucial importance to the channel quality in terms of DCN and BER.

Chapter 6

Conclusion

The thesis presented an investigation on receiver algorithms for OFDM in correlated channels. In chapter 3, equations for equalizers used in SISO, SIMO and MIMO with and without SMUX have been derived and compared by BER simulations. The equalizer chosen for further use in the following chapters was the MMSE receiver with ordered successive interference cancellation. The MMSE-OSIC provides a good balance between computational efficiency and equalization performance in the Rayleigh channels used for the simulations.

After a review of the aforementioned receiver algorithms, the focus was brought to channel coding, specifically to coding in LTE. Turbo coding and rate matching have been investigated. Simulations showed that the performance increases when the transmitter and the receiver are equipped with multiple antennas, and that STBC outperforms SMUX in the low SNR regime.

Chapter 5 presented a study of spatially correlated channels. The analysis furthermore touched the WINNER II channel model, which is the most sophisticated channel model available today. A deterministic, geometrically based channel model was also developed to investigate the invertibility of the channel matrix in a controlled environment. Fading was added to the model to enable a comparison to the WINNER II model, showing that the WINNER II model achieves performance from a higher spatial resolvability, because of the cluster-based approach in the model. Furthermore, simulations of throughput showed an additional advantage of utilizing STBC compared to SMUX in the low SNR regime, when the channel is badly conditioned.

From this thesis, what can be concluded is that multiple antennas at the transmitter and the receiver increase the throughput; because of an additional diversity gain in the low SNR regime, and because of spatial multiplexing in the high SNR regime. It is seen that when using highly correlated channels, the importance of using STBC in the low SNR regime is even higher, as SMUX throughput suffers from a significant negative power gain. STBC throughput, on the other hand, only loses a small amount of diversity gain under the same channel conditions.

Bibliography

[1] N. Costa and S. Haykin, *Multiple-Input Multiple-Output Channel Models: Theory and Practice*. John Wiley & Sons, 2010.

[2] J. Simkin. (2012, Mar.) Sparcatus educational - wireless telegraphy. [Online]. Available: http://www.spartacus.schoolnet.co.uk/FWWairwireless.htm

[3] M. Katzdorn. (2012, Mar.) Edwin h. armstrong. [Online]. Available: http://users.erols.com/oldradio/

[4] Wikipedia. (2012, Mar.) Johnson–nyquist noise. [Online]. Available: http://en.wikipedia.org/wiki/Johnson%E2%80%93Nyquist_noise

[5] J. G. Proakis and M. Salehi, *Digital Communications*. Mcgraw-Hill, 2008.

[6] P. Morgensen, "Gsm base-station antenna diversity using soft decision combining on up-link and delayed-signal transmission on down-link," in *Vehicular Technology Conference, 1993., 43rd IEEE*, may 1993, pp. 611 –616.

[7] D. Brennan, "Linear Diversity Combining Techniques," *Proceedings of the IRE*, vol. 47, no. 6, pp. 1075–1102, Jun. 1959.

[8] S. Alamouti, "A simple transmit diversity technique for wireless communications," *Selected Areas in Communications, IEEE Journal on*, vol. 16, no. 8, pp. 1451 –1458, oct 1998.

[9] C.-J. Kim, Y.-S. Kim, and C.-Y. Jung, "Ber analysis of qam with mrc space diversity in rayleigh fading channel," in *Personal, Indoor and Mobile Radio Communications, 1995. PIMRC'95. 'Wireless: Merging onto the Information Superhighway'., Sixth IEEE International Symposium on*, vol. 2, sep 1995, pp. 482 –485 vol.2.

[10] A. van Zelst, "MIMO OFDM for Wireless LANs," Ph.D. dissertation, Technische Universiteit Eindhoven, 2004.

[11] D. Tse and P. Viswanath, *Fundamentals Of Wireless Communication*. Cambridge University Press, 2005.

[12] P. Liu and I.-M. Kim, "Exact and closed-form error performance analysis for hard mmse-sic detection in mimo systems," *Communications, IEEE Transactions on*, vol. 59, no. 9, pp. 2463 –2477, september 2011.

[13] B. Vucetic and J. Yuan, *Turbo Codes: Principles and Applications.* Kluwer Academic Publishers, 2000.

[14] 3GPP, "Evolved Universal Terrestrial Radio Access (E-UTRA); Multiplexing and channel coding," 3rd Generation Partnership Project (3GPP), TS 36.212, Sep. 2008. [Online]. Available: http://www.3gpp.org/ftp/Specs/html-info/36212.htm

[15] S. Sesia, I. Toufik, and M. Baker, *LTE-the UMTS Long Term Evolution : from theory to practice 2nd ed.* Wiley, 2011.

[16] F. Tosato and P. Bisaglia, "Simplified soft-output demapper for binary interleaved cofdm with application to hiperlan/2," in *Communications, 2002. ICC 2002. IEEE International Conference on*, vol. 2, 2002, pp. 664 – 668 vol.2.

[17] Mathworks. (2012, May) Digital modulation, exact llr algorithm. [Online]. Available: http://www.mathworks.se/help/toolbox/comm/ug/fp59183.html#brc6yjx

[18] Alcatel-Lucent, "DL E-UTRA Performance Checkpoint, 3GPP R1-071967," 3rd Generation Partnership Project (3GPP), TR R1-071967, april 2007. [Online]. Available: http://www.3gpp.org/ftp/tsg_ran/WG1_RL1/TSGR1_AH/LTE_Performance_evaluation_April-07/Docs/R1-071967.zip

[19] M. Herdin, G. Gritsch, B. Badic, and E. Bonek, "The influence of channel models on simulated mimo performance," in *Vehicular Technology Conference, 2004. VTC 2004-Spring. 2004 IEEE 59th*, vol. 1, may 2004, pp. 304 – 307 Vol.1.

[20] M. Ozcelik, N. Czink, and E. Bonek, "What makes a good mimo channel model?" in *Vehicular Technology Conference, 2005. VTC 2005-Spring. 2005 IEEE 61st*, vol. 1, may-1 june 2005, pp. 156 – 160 Vol. 1.

[21] P. Kyösti, J. Meinilä, L. Hentilä, X. Zhao, T. Jämsä, C. Schneider, M. Narandzić, M. Milojević, A. Hong, J. Ylitalo, V.-M. Holappa, M. Alatossava, R. Bultitude, Y. de Jong, and T. Rautiainen, "WINNER II Channel Models," EC FP6, Tech. Rep., Sep. 2007. [Online]. Available: http://www.ist-winner.org/deliverables.html

[22] L. Hentilä, P. Kyösti, M. Käske, M. Narandzic, and M. Alatossava. (2007, Dec.) Matlab implementation of the winner phase ii channel model ver1.1. [Online]. Available: http://www.ist-winner.org/phase_2_model.html

[23] R. W. Heath, Jr., and A. J. Paulraj, "Diversity versus multiplexing in narrowband mimo channels: A tradeoff based on euclidean distance," 2001.

Appendix A

BER derivations

A.1 BER in AWGN

A.1.1 BER for BPSK

To derive the SER of any phase modulated signal, the following general equation can be utilized[5, eq. (4.1-15)]

$$P_s = \sum_{m=1}^{M} P_m P_{s,m} \tag{A.1}$$

$$P_{s,m} = \sum_{\substack{1 \le m' \le M \\ m' \neq m}} \int_{D_{m'}} p(\hat{d}|d_m)dr \tag{A.2}$$

in which the probability that a symbol is wrongly decoded as a symbol belonging to another region ($D_{m'}$) is derived. The equation is weighted by the probability that the given symbol (P_m) is transmitted. In this project, the probability P_m equals $1/M$ for all symbols, as random data is used for transmission.

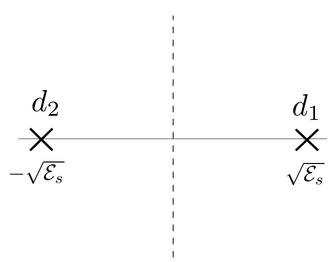

(a) 2-PSK

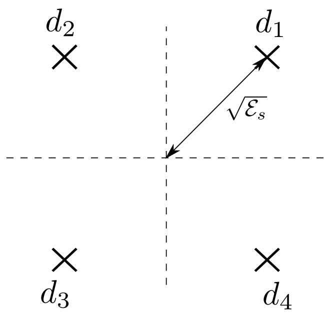

(b) 4-PSK

Figure A.1: Position and decision boundaries for BPSK (a) and QPSK (b) constellations.

For BPSK, the symbols are defined as in figure A.1(a) with an equal distribution of symbol appearances. Since noise on the imaginary axis cannot influence the demodulation of BPSK, the SER can be derived as

$$P_{s,\mathrm{BPSK}} = \frac{1}{2}\int_{-\infty}^{0} p(\hat{d}|\sqrt{\mathcal{E}_s})dr + \frac{1}{2}\int_{0}^{\infty} p(\hat{d}|-\sqrt{\mathcal{E}_s})dr \tag{A.3}$$

$$= \frac{1}{2}\mathrm{P}\left[\mathcal{N}\left(\sqrt{\mathcal{E}_s}, \frac{\sqrt{N_0}}{2}\right) < 0\right] + \frac{1}{2}\mathrm{P}\left[\mathcal{N}\left(-\sqrt{\mathcal{E}_s}, \frac{\sqrt{N_0}}{2}\right) > 0\right]. \tag{A.4}$$

Now, the Q-function which, on base of the PDF[1] of the Gaussian distribution, is defined as[5, eq. (2.3-10)]

$$Q(x) = \mathrm{P}\left[\mathcal{N}(0,1) > x\right] = \frac{1}{\sqrt{2\pi}}\int_{x}^{\infty} e^{-\frac{t^2}{2}}dt, \tag{A.5}$$

which induces

$$\mathrm{P}[X > x] = Q\left(\frac{x-\mu}{\sigma}\right) \tag{A.6}$$

and

$$\mathrm{P}[X < x] = Q\left(\frac{\mu-x}{\sigma}\right) \tag{A.7}$$

can be substituted into (A.4) so that the SER can be derived to

$$P_{s,\mathrm{BPSK}} = \frac{1}{2}Q\left(\frac{\sqrt{\mathcal{E}_s}-0}{\sqrt{\frac{N_0}{2}}}\right) + \frac{1}{2}Q\left(\frac{0-(-\sqrt{\mathcal{E}_s})}{\sqrt{\frac{N_0}{2}}}\right) \tag{A.8}$$

$$= Q\left(\sqrt{\frac{2\mathcal{E}_s}{N_0}}\right). \tag{A.9}$$

Since BPSK carries only one bit per symbol, the BER equals the SER $P_{b,\mathrm{BPSK}} = P_{s,\mathrm{BPSK}}$.

A.1.2 BER for QPSK

Since equation (A.1) defines the SER for every phase and amplitude modulation, it obviously includes QPSK. However, due to the fact that $P_{s,1} = P_{s,2} = P_{s,3} = P_{s,4}$, because of the equal distribution of the symbols in the constellation diagram in figure A.1(b),

$$P_{s,\mathrm{QPSK}} = \sum_{m=1}^{4} P_m \cdot P_{s,m} \tag{A.10}$$

$$= 4 \cdot \frac{1}{4}P_{s,m}$$

$$= P_{s,m}, \tag{A.11}$$

[1]Probability Density Function

meaning that (A.2) must be derived to find the SER for QPSK.

When calculating the integral in equation (A.2), the probability must be evaluated for two decision rules; one along the real axis and one along the imaginary axis. The mean of the Gaussian distribution in the following is the energy of the signal transposed to the real and imaginary axis, thus the probability that a transmitted symbol d_1 will be demodulated as d_2 is calculated as

$$
\begin{aligned}
P_{s,1-2} &= \int_{D_2} p(\hat{d}|d_1)dr && \text{(A.12)} \\
&= \mathrm{P}\left[\mathcal{N}\left(\cos\left(\frac{\pi}{4}\right)\sqrt{\mathcal{E}_s}, \frac{N_0}{2}\right) < 0 \cap \mathcal{N}\left(\sin\left(\frac{\pi}{4}\right)\sqrt{\mathcal{E}_s}, \frac{N_0}{2}\right) > 0\right] \\
&= Q\left(\frac{\cos\left(\frac{\pi}{4}\right)\sqrt{\mathcal{E}_s} - 0}{\sqrt{\frac{N_0}{2}}}\right) \cdot Q\left(\frac{0 - \sin\left(\frac{\pi}{4}\right)\sqrt{\mathcal{E}_s}}{\sqrt{\frac{N_0}{2}}}\right) \\
&= Q\left(\sqrt{\frac{\mathcal{E}_s}{N_0}}\right) \cdot Q\left(-\sqrt{\frac{\mathcal{E}_s}{N_0}}\right) && \text{(A.13)}
\end{aligned}
$$

because the symbol s_1 has an angle of $45° = \pi/4$. In the same way, s_{1-3} is calculated as

$$
\begin{aligned}
P_{s,1-3} &= \int_{D_2} p(\hat{d}|d_1)dr && \text{(A.14)} \\
&= \mathrm{P}\left[\mathcal{N}\left(\cos\left(\frac{\pi}{4}\right)\sqrt{\mathcal{E}_s}, \frac{N_0}{2}\right) < 0 \cap \mathcal{N}\left(\sin\left(\frac{\pi}{4}\right)\sqrt{\mathcal{E}_s}, \frac{N_0}{2}\right) < 0\right] \\
&= Q\left(\frac{\cos\left(\frac{\pi}{4}\right)\sqrt{\mathcal{E}_s} - 0}{\sqrt{\frac{N_0}{2}}}\right) \cdot Q\left(\frac{\sin\left(\frac{\pi}{4}\right)\sqrt{\mathcal{E}_s} - 0}{\sqrt{\frac{N_0}{2}}}\right) \\
&= Q\left(\sqrt{\frac{\mathcal{E}_s}{N_0}}\right) \cdot Q\left(\sqrt{\frac{\mathcal{E}_s}{N_0}}\right). && \text{(A.15)}
\end{aligned}
$$

By remembering that $P_{s,1-2} = P_{s,1-4}$, due to the identical distribution of the constellation points, the equation for $P_{s,1}$ reduces to

$$
\begin{aligned}
P_{s,1} &= 2 \cdot \int_{D_2=D_4} p(\hat{d}|d_1)dr + \int_{D_3} p(\hat{d}|d_1)dr && \text{(A.16)} \\
&= 2 \cdot Q\left(\sqrt{\frac{\mathcal{E}_s}{N_0}}\right) \cdot Q\left(-\sqrt{\frac{\mathcal{E}_s}{N_0}}\right) + Q\left(\sqrt{\frac{\mathcal{E}_s}{N_0}}\right) \cdot Q\left(\sqrt{\frac{\mathcal{E}_s}{N_0}}\right).
\end{aligned}
$$

The BER equation for $P_{s,\mathrm{QPSK}}$ equals that for $P_{s,1}$ since the noise is Gaussian with zero mean and the symbols are identically distributed.

For QPSK, the BER does not equal the SER, since each symbol represents two bits. In this project, a grey encoded constellation will be used. This means that a detection error might only introduce 1 half symbol error, giving

$$
P_{b,\mathrm{QPSK}} = \frac{1}{2} 2 \cdot Q\left(\sqrt{\frac{\mathcal{E}_s}{N_0}}\right) \cdot Q\left(-\sqrt{\frac{\mathcal{E}_s}{N_0}}\right) + Q\left(\sqrt{\frac{\mathcal{E}_s}{N_0}}\right) \cdot Q\left(\sqrt{\frac{\mathcal{E}_s}{N_0}}\right) \tag{A.17}
$$

which reduces to

$$P_{b,\text{QPSK}} = Q\left(\sqrt{\frac{\mathcal{E}_s}{N_0}}\right). \tag{A.18}$$

A.1.3 BER for M-QAM

The SER of a M-QAM constellation can also be derived from equation (A.1). Because of the unequal distribution of the symbols in a M-QAM constellation, the derived BER is not the same for all symbols and must for this reason be calculated per symbol. For the verification of M-QAM simulations, the following general M-QAM SER approximation will be used[5, eq. (4.3-30)]:

$$\begin{aligned}P_{s,\text{M-QAM}} \simeq\ & 4\left(1-\frac{1}{\sqrt{M}}\right)\cdot Q\left(\sqrt{\frac{3k}{M-1}\frac{\mathcal{E}_{b\text{avg}}}{N_0}}\right)\ldots\\ &\cdot\left(1-\left(1-\frac{1}{\sqrt{M}}\right)\cdot Q\left(\sqrt{\frac{3k}{M-1}\frac{\mathcal{E}_{b\text{avg}}}{N_0}}\right)\right)\end{aligned} \tag{A.19}$$

with k being the number of bits per symbol and $M = 2^k$ being the number of symbols in the constellation. Note that since the modulation form is not constant in amplitude, $\mathcal{E}_{b\text{avg}}$ is used to define the average energy per bit when all symbols are transmitted with equal probability.

For 16-QAM, equation (A.19) reduces to

$$P_{s,\text{16-QAM}} \simeq 3Q\left(\sqrt{\frac{4}{5}\frac{\mathcal{E}_{b\text{avg}}}{N_0}}\right)\cdot\left(1-\frac{3}{4}Q\left(\sqrt{\frac{4}{5}\frac{\mathcal{E}_{b\text{avg}}}{N_0}}\right)\right). \tag{A.20}$$

A similar equation can be derived for 64-QAM.

When considering high $\mathcal{E}_s/N_0$, it can be assumed that only one bit error occurs for each symbol error in a gray mapped symbol constellation. For this reason,

$$\begin{aligned}P_{b,\text{16-QAM}} &\simeq \frac{1}{k}P_{s,\text{16-QAM}}\\ &\simeq \frac{3}{4}Q\left(\sqrt{\frac{4}{5}\frac{\mathcal{E}_{b\text{avg}}}{N_0}}\right)\cdot\left(1-\frac{3}{4}Q\left(\sqrt{\frac{4}{5}\frac{\mathcal{E}_{b\text{avg}}}{N_0}}\right)\right).\end{aligned} \tag{A.21}$$

The validity of this assumption is shown in section 3.1.1.

A.2 BER in a frequency-nonselective Rayleigh environment

Section A.1.1 shows the derivations of the theoretical BER for BPSK in an AWGN environment. Now this derivation will be extended to comply with the signal model in equation (3.6). In the following, it is assumed that the phase change ϕ is detected and corrected in the receiver and that the amplitude α is estimated. The SNR γ then can be defined as

$$\gamma_s = \frac{\mathcal{E}_s}{N_0}\alpha^2, \tag{A.22}$$

which induces

$$P_b(\gamma_s) = Q\left(\sqrt{2\gamma_s}\right) \tag{A.23}$$

for BPSK when using the derivation in section A.1.1.

When α is Rayleigh distributed, α^2 and therefore also γ_s will have a Chi-squared distribution with two degrees of freedom. Recall that the PDF for a Chi-squared distribution with two degrees of freedom is defined as

$$p(x) = \frac{1}{2\sigma^2}e^{-x/2\sigma^2} \qquad \text{for} \quad x > 0 \tag{A.24}$$

with

$$\mathrm{E}[\gamma_s] = 2\sigma^2. \tag{A.25}$$

The average SNR $\bar{\gamma_s}$ then is

$$\bar{\gamma_s} = \mathrm{E}[\gamma_s] = \frac{\mathcal{E}_s}{N_0}\mathrm{E}\left[\alpha^2\right], \tag{A.26}$$

which can be inserted into the PDF of the distribution, thus giving

$$p(\gamma_s) = \frac{1}{\bar{\gamma_s}}e^{-\gamma_s/\bar{\gamma_s}} \qquad \text{for} \quad \gamma > 0. \tag{A.27}$$

To calculate the BER in the Rayleigh environment, the BER calculated for AWGN must be evaluated for all γ as

$$P_b = \int_0^\infty P_b(\gamma_s)p(\gamma_s)d\gamma_s, \tag{A.28}$$

which for BPSK reduces to

$$P_{b,\mathrm{BPSK}} = \frac{1}{2}\left(1 - \sqrt{\frac{\bar{\gamma_s}}{1+\bar{\gamma_s}}}\right). \tag{A.29}$$

For QPSK, the equation reduces instead to

$$P_{b,\mathrm{QPSK}} = \frac{1}{2}\left(1 - \sqrt{\frac{\bar{\gamma_s}}{2+\bar{\gamma_s}}}\right). \tag{A.30}$$

A.3 BER in receive diversity

In this section, the BER for QPSK with multiple antennas will be derived. The narrowband channels are assumed to be uncorrelated in space and affected by Rayleigh fading.

As the basis for this derivation, the equation for BER for SISO in an AWGN channel as

$$P_b = Q\left(\sqrt{\frac{\mathcal{E}_s}{N_0}}\right) \tag{A.31}$$

derived in section A.1.2 is utilized. This equation will be used in equation (A.28) - the equation for calculation BER in fading channels. As scaling function $p(\gamma)$ in equation (A.28), a Chi-Squared distribution, which is the sum of L squared normal distributed variables with $L = 2R$ degrees of freedom, must be utilized, since

$$\mathrm{E}\left[h^2\right] = \sum_{r=1}^{R} h_r^2 = \sum_{r=1}^{R} \left(X_{r,1}^2 + X_{r,2}^2\right) \tag{A.32}$$

when using MRC, with $X_{r,n}$ being uncorrelated Gaussian distributed random variables.

The Chi-Squared distribution with $R = 2L$ degrees of freedom is defined as

$$p(\gamma_s) = \frac{1}{(R-1)!\overline{\gamma}_s^R}\gamma^{R-1}e^{-\gamma_s/\overline{\gamma}_s} \tag{A.33}$$

$$\overline{\gamma}_s = \frac{\mathcal{E}_s}{N_0}\mathrm{E}\left[\alpha_k^2\right]. \tag{A.34}$$

When utilizing equation (A.28) on (A.31) and (A.33), the BER for QPSK with N_{Rx} number of receive antennas can be written as[5, eq. 13.4-15]

$$P_{b,\mathrm{QPSK}} = \left(\frac{1}{2}(1-\mu)\right)^{N_{\mathrm{Rx}}} \sum_{r=0}^{N_{\mathrm{Rx}}-1} \binom{N_{\mathrm{Rx}}-1+r}{r} \left(\frac{1}{2}(1+\mu)\right)^{r} \tag{A.35}$$

$$\mu = \sqrt{\frac{\overline{\gamma}_s}{1+\overline{\gamma}_s}} \tag{A.36}$$

For M-QAM verifications, the derivations in [9] is used.

Appendix B

Orthogonal Frequency Division Multiplexing

In this appendix, a short description of OFDM will be provided, after which the BER of OFDM modulated signals will be derived.

The purpose of dividing information into several carrier frequencies with a slower symbol rate is to diminish time delays caused by multipath. By lowering the symbol rate, the effect of ISI can be reduced or, by using a CP longer than the maximum channel delay, eliminated. The idea of OFDM is to divide the available channel bandwidth into several narrow bandwidth subchannels. When keeping an exact distance of $\Delta f = 1/T_s$ between the subcarriers, orthogonality is obtained. This can be proved by showing that

$$\int_0^T \cos(2\pi k_1 \Delta f)\cos(2\pi k_2 \Delta f)dt = 0 \qquad \text{for} \qquad k_1 \neq k_2, \tag{B.1}$$

which is true when k is an integer. The frequency spectrum of the transmitted signal is then as shown in figure B.1, which clearly shows that only energy from a particular subcarrier itself is present at the center frequency of a subcarrier. If the channel is estimated inaccurately, or the channel varies thoughout one symbol time, the orthogonality will be lost, resulting in ICI[1].

An OFDM symbol is created by doing a IDFT of a number of M-PSK or M-QAM modulated data symbols. To eliminate ISI, a CP is created by placing a copy of the last part of the OFDM symbol prior to the OFDM symbol before transmitting.

In order to describe the OFDM modulation and transmission, it is convenient to define the discrete Fourier matrix

$$\Psi_{N_{\text{dft}}} = \frac{1}{\sqrt{N_{\text{dft}}}}\psi_{k,l} \qquad \text{for} \qquad k,l = 0,1,...,N_{\text{dft}}-1 \tag{B.2}$$

$$\psi_{k,l} = e^{-\frac{j2\pi kl}{N_{\text{dft}}}} \tag{B.3}$$

[1]Inter Carrier Interference

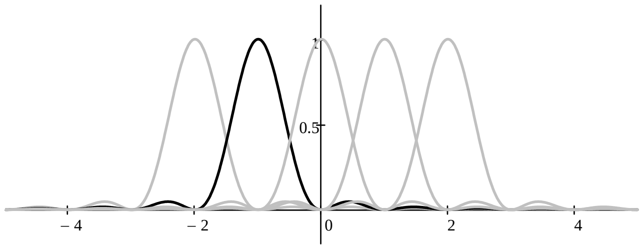

Figure B.1: A transmission with OFDM modulated symbols at a symbol rate of 1. Notice that only energy of the particular subcarrier is present at its center.

with N_{dft} being the DFT size. The matrix normalization by $\sqrt{N_{\text{dft}}}$ is introduced to preserve the same energy in the time and frequency domain. Using Ψ, Ψ_{mod}, with dimensions $(N_{\text{ofdm}} = N_{\text{dft}} + N_{\text{cp}}) \times N_{\text{dft}}$ is defined as a IDFT, which includes the CP. Therefore, a set of OFDM symbols $\mathbf{S}$ of dimension $N_{\text{ofdm}} \times N_{\text{block}}$ can be expressed as

$$\mathbf{S} = \Psi_{\text{mod}}\mathbf{D}, \tag{B.4}$$

where D is the matrix describing the original set of symbols. For demonstration, a modulation matrix for a dimension of 6×4 is seen here:

$$\Psi = \frac{1}{\sqrt{N_{dft}}} \begin{pmatrix} \psi_{1,1} & \psi_{1,2} & \psi_{1,3} & \psi_{1,4} \\ \psi_{2,1} & \psi_{2,2} & \psi_{2,3} & \psi_{2,4} \\ \psi_{3,1} & \psi_{3,2} & \psi_{3,3} & \psi_{3,4} \\ \psi_{4,1} & \psi_{4,2} & \psi_{4,3} & \psi_{4,4} \end{pmatrix} \tag{B.5}$$

$$\Psi_{\text{mod}} = \begin{pmatrix} 0 & 0 & 1 & 0 \\ 0 & 0 & 0 & 1 \\ 1 & 0 & 0 & 0 \\ 0 & 1 & 0 & 0 \\ 0 & 0 & 1 & 0 \\ 0 & 0 & 0 & 1 \end{pmatrix} \cdot \Psi^{-1} = \frac{1}{2} \cdot \begin{pmatrix} 1 & -1 & 1 & -1 \\ 1 & -j & -1 & j \\ 1 & 1 & 1 & 1 \\ 1 & j & -1 & -j \\ 1 & -1 & 1 & -1 \\ 1 & -j & -1 & j \end{pmatrix}. \tag{B.6}$$

The matrix $\mathbf{S}$, after OFDM modulation, is converted into a vector $\mathbf{s}$ of length $N_{\text{ofdm}} \cdot N_{\text{block}}$ by a column by column transformation, transmitted and affected by the channel. That is,

$$\mathbf{r} = g\mathbf{s} + \widetilde{\mathbf{n}} \tag{B.7}$$

with $\widetilde{\mathbf{n}}$ being a vector with the size of $\mathbf{s}$, but containing Gaussian noise. The channel is considered constant throughout a symbol time.

At the receiver side, an entire frame is changed to a matrix $\mathbf{R}$ of the same dimension as $\mathbf{S}$. Then the CP is removed and the frame is transformed to the frequency domain by

$$\mathbf{Y} = \Psi_{\text{demod}}\mathbf{R}, \tag{B.8}$$

where Ψ_{demod} is a $N_{\text{dft}}, N_{\text{ofdm}}$ matrix with the lower square part being a DFT matrix and the upper part padded with zeros. For demonstration, a 6×4 demodulation matrix would look like

$$\Psi_{\text{demod}} = \frac{1}{\sqrt{N_{\text{dft}}}} \begin{pmatrix} 0 & 0 & 0 & 0 \\ 0 & 0 & 0 & 0 \\ 1 & 0 & 0 & 0 \\ 0 & 1 & 0 & 0 \\ 0 & 0 & 1 & 0 \\ 0 & 0 & 0 & 1 \end{pmatrix} \cdot \Psi = \frac{1}{2} \cdot \begin{pmatrix} 0 & 0 & 0 & 0 \\ 0 & 0 & 0 & 0 \\ 1 & 1 & 1 & 1 \\ 1 & -j & -1 & j \\ 1 & -1 & 1 & -1 \\ 1 & j & -1 & -j \end{pmatrix}. \tag{B.9}$$

B.1 BER of OFDM in Rayleigh fading environment

The principle behind OFDM is to have several symbols with a lower symbol rate and consequently a lower bandwidth placed at orthogonal frequencies. The SNR of these symbols is

$$SNR = \frac{\mathcal{E}_s}{N_0 BT} \tag{B.10}$$

with T being the symbol time, and B being the symbol bandwidth. Since the bandwidth $B = {}^1\!/_T$ for M-PSK and M-QAM, the SNR equation reduces to

$$SNR = \frac{\mathcal{E}_s}{N_0} \tag{B.11}$$

which equals the SNR for single carrier modulation.

Appendix C

Metric for channel quality

Working with correlation creates a demand of a metric of the channel quality for use in SMUX. In mathematics, CN[1] is commonly known to measure the stability of the matrix, that is, how much the outcome can change due to small changes in the argument. Traditionally, this has referred to numeric quantization, but AWGN or inaccurate channel estimations in MIMO affect the argument in the same way. When using OFDM in a wideband channel, the CN is calculated per subcarrier, indicating the capability for SMUX at each subcarrier.

Several CN definitions have been suggested:

- 2-norm CN: $||\mathbf{H}||_2 \cdot \left|\left|\mathbf{H}^{-1}\right|\right|_2$,
- Frobenius-norm CN: $||\mathbf{H}||_\mathrm{F} \cdot \left|\left|\mathbf{H}^{-1}\right|\right|_\mathrm{F}$,
- Demmel CN: $||\mathbf{H}||_\mathrm{F} \cdot \left|\left|\mathbf{H}^{-1}\right|\right|_2$.

The 2-norm of a matrix $||\mathbf{H}||_2$ is equal to the largest singular value of the matrix σ_max, while the 2-norm of the inverse matrix $||\mathbf{H^{-1}}||_2 = \sigma_\mathrm{min}^{-1}$ and $||\mathbf{H}||_\mathrm{F} = \sqrt{\sum_i \sigma_i^2}$.

Most literature uses the 2-norm CN as condition metric for MIMO channels[23, p. 2], but some literature suggests the DCN as a better metric when evaluating MIMO channels, since all singular values then are taken into consideration. The DCN will be used in this project.

C.1 Relation between BER and DCN

In this section, it will be investigated whether it is possible to derive a relation between BER and the condition number of a given channel realization.

In figure C.1, the relation between SNR and DCN is shown. It is seen that a linear relationship between DCN and SNR in the rate of approximately

[1] Condtion Number

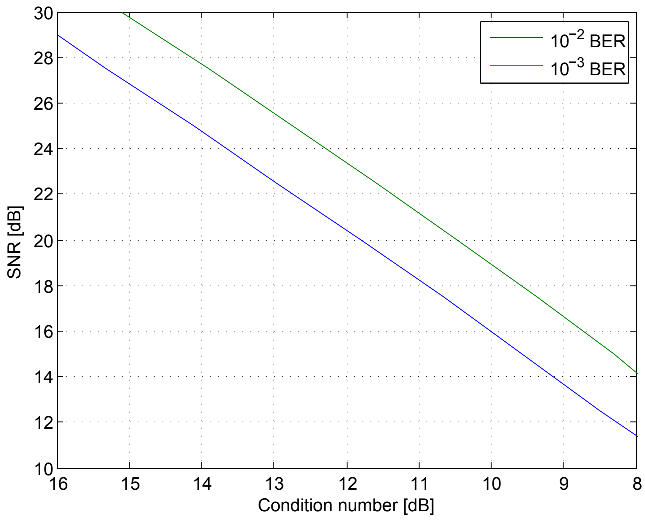

Figure C.1: SNR/DCN relation with a MMSE-OSIC receiver in 2×2 channel with 16-QAM modulation

2.2 dB SNR to 1 dB DCN exists. This relation can be utilized to do a rough prediction of the BER in a correlated MIMO channel from the BER of a i.i.d. channel model by compensating for the power loss caused by a channel with a high DCN. It is important to mention that some deviation from this relationship occurs if the received energy from each transmitted stream differs.

Appendix D

Link simulator

During this project, a MATLAB link simulator has been developed to support the BER derivations and receiver efficiencies. In this appendix, this simulator will be described.

Parameter	Desciption
`SNR_start`	First SNR test point, provided in dB
`SNR_stop`	Last SNR test point, provided in dB
`I`	Number of SNR simulation points
`J`	Minimum number of errors before continuing to next SNR
`J_min`	Maximum number of iterations per simulation
`J_max`	Maximum number of iterations per simulation
`O`	OFDM symbols per block
`K`	Data symbols per OFDM symbol
`N`	Samples per data symbol
`P`	Length of CP in samples
`T`	No of Tx antennas
`R`	No of RX antennas
`Channel`	Channel-specific properties
`M`	Number of points in constallation: BPSK, QPSK, 16-QAM, 64-QAM is supported
`CR`	Code rate (set to 1 to disable Turbo coding)
`SNR_type`	1: SNR per bit, 2: SNR per symbol
`Mod_type`	1: Normal modulation, 2: Alamouti time-based modulation (Only for T=2)
`Equal_type` (spatial multiplexing)	1: ZF, 2: MMSE, 3: ZF-SIC, 4: MMSE-SIC, 5: ZF-OSIC, 6: MMSE-OSIC, 7: ML
`Equal_type` (diversity)	1: Selection Combining, 2: Selection Combining per subcarrier, 3: Maximum Ratio Combining

Table D.1: Configuration parameters in MATLAB simulator

The simulator consists of a master file `multitest.m`, in which the parameters of the simulation are configured. It is possible to run multiple tests looping the main simulation function `main()` with different sets of parameters. One test is to sweep over a predefined SNR range. In table D.1 the complete set of configurable variables is specified.

The structure array `Channel` must be configured with channel-specific properties. `Channel{1}` is always configured to the channel type to be used in the current simulation. Possible channel types include AWGN (no fading), uncorrelated Rayleigh fading, Rayleigh fading with Van Zelst correlation, COST207 channel models, WINNER II, and Sandbox model with and without the geometric extension. The detailed configuration options are found in `multitest.m`. The simulator includes functions to plot the outcome of the simulations in terms BER (`plotsnrber()`) and throughput (`plotthrsnr()`) with respect to SNR and condition number.

D.1 main()

This function contains the structure of the simulator itself. It finds the uncoded BER, the coded BER, and the resulting throughput for each defined SNR point with the parameters defined in `multitest`. The structure of `main()` is shown in listing D.1. The code uses the `parfor` loop from the Parallel Computing toolbox in MATLAB to gain benefit from multi-core computers. An array of sizes `{i,J_max+1}` is returned by the function.

```
for i=1:I
  NumErrs = 0;
  parfor j=1:J_max
    GenerateAndEncode();
    Modulate();
    OFDM_modulate();
    ChannelAffect();
    OFDM_demodulate();
    Equalize();
    Demodulate();

    Errs(i,j) = DecodeAndCompare();
    SumErrs = SumErrs + NumErrs(i,j);
    ConsoleWriteProgress();
    if j == J_max || (SumErrs >= J && j > J_min)
      break;

return NumErrs;
```

Listing D.1: `siso_ofdm()` structure

The console output of `main()` typically is, as shown in D.2. The dots show the progress for the calculation in each SNR point. If extrapolation reveals that the maximum number of runs (`J_max`) will be reached before the number of errors wanted (`J`), the dots are replaced with commas to indicate a potential decrease of precision in logarithmic BER plots.

```
Calculating for 0 dB SNR
........................................
Calculating for 5 dB SNR
........................................
Calculating for 10 dB SNR
.................................,,,,,,,
Calculating for 15 dB SNR
...,,,,,,,,,,,,,,,,,,,,,,,,,,,,,,,,,,,,,
```

Listing D.2: `main()` console output.

D.2 plotsnrber()

The results of multiple tests can be plotted with BER in respect to SNR graph, using `plotsnrber()`. It is possible to store simulations by saving the workspace, and then load them prior to calling this function. One simulation point in the graph can be clicked to see the accumulated average of the BER point to check whether the simulation seems to have converged. If the simulation is run with Turbo coding and rate matching enabled, the coded BER is shown as a dashed line.

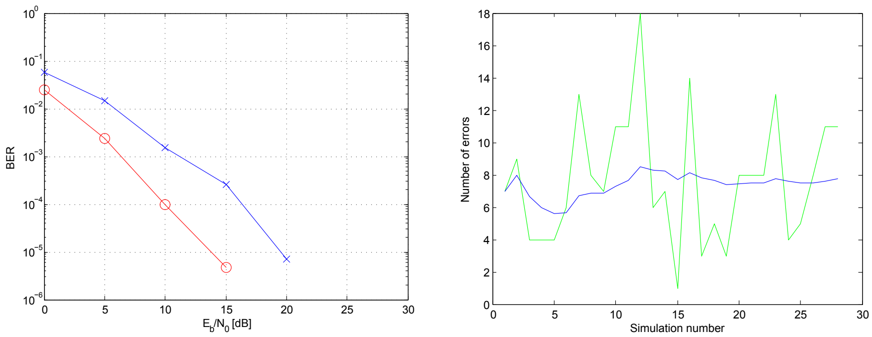

(a) Simulation plot **(b)** Convergence plot

Figure D.1: In (a), a random simulation figure, generated by `plotsnrber()` is shown. In (b), a convergence plot of a single simulation point is shown.

In figure D.1(a), a random simulation output is shown. The simulation is run with the parameters `J = 200` and `J_max = 130`. In figure D.1(b), a convergence plot, which is created by clicking a particular simulation point in figure D.1(a) is shown. The green line illustrates the number of errors per loop in the simulation, while the blue line shows accumulated mean error rate.

D.3 plotdcnsnr()

Simulations with varying DCN created a demand to see the relation between SNR and DCN. The function interpolates lines between DCN points for each SNR in a simulation with varying SNR and DCN, and finds the crossings with the defined BER (typically 10^{-2}, 10^{-3}). A plot is then created with SNR and DCN on the axes. The outcome of the function is shown in figure C.1.

D.4 plotthrsnr()

To evaluate channel coding, the throughput as a function of SNR can be plotted by using the function `plotthrsnr()`. The function draws a line for each simulated code rate, and returns the maximum throughput over all code rates for each SNR point.